Commentary on API 653 Settlement Methods

Draft copy – dated August 5, 2022

Authored by PEMY Consulting LLC.

Philip E. Myers

George G. Woodworth

Andy Wong

Introduction 1
Settlement and Failure Mechanisms 3
Basic Settlement Modes 4
Cosine Curves of Higher Modes 12
API 653 Differential Settlement Analysis 17
References 39
Figures 39
Appendix A. Commentary on the Marr Method 41

DRAFT

Introduction

Fortunately, tanks are relatively flexible structures and can tolerate a surprisingly large amount of settlement without showing signs of distress. The rate of reported incidents involving settlement problems confirms this. However, the forgiveness of steel flexibility is not without limits. There are numerous examples of tank failures that have resulted in inoperative floating roofs, shell and roof buckling damage, leaks, and, at worst, a catastrophic and complete loss of tank contents. When settlement failures occur, they tend to be serious since they often can discharge the entire tank contents.

The complete elimination of settling is neither possible nor necessary. This section is about determining how much can be tolerated – that's key. Foundation design, soil conditions, tank geometry and loading, and drainage all have a significant effect on settlement. Large petroleum tanks are generally constructed on compacted soil foundations or granular material. Concrete ringwall foundations are also often used. Smaller tanks in the chemical industry are often constructed on concrete slabs. Even with reinforced slabs and ringwalls there will be some global and local settlement of the tank bottom.

This chapter applies primarily to settlement of large tanks over 50 ft in diameter constructed on compacted soil or ringwall foundations. The reason for this is that most of these tanks are constructed on compressible foundations where the thickness, elasticity, and compressibility of the foundation and subsoil layers can vary enough to produce nonplanar distortions with the application of uniform loading. However, the basic principles apply to all tanks, especially uniform settling and planar tilt.

The foundation loading pattern under static conditions is such that when filled, tanks will uniformly load the foundation beneath the tank as the result of hydrostatic pressure in a disk pattern. The edge of the tank under the shell, however, has increased loading due to the weight of the shell and the part of the roof supported by it. It also has other local loading effects such as twisting of the plates under the shell due to shell rotation. The edge of the foundation is also unlike the interior areas because it terminates near the outside of the tank and is often constructed of materials other than those of the interior (ringwall, etc.). This also allows for different soil properties such as moisture and compaction under the tank and outside its footprint, which promotes nonuniform settlement.

For these reasons a significant portion of the foundation and settlement problems occur at the outside edge of the foundation. In fact, the only assessment that can be made with regard to settling without entering the interior of the tank is the elevation readings made at the base of the tank. Since most tanks are not taken out of service for a decade or more, it is advantageous that one key indicator of settlement (elevation monitoring at tank base) is also the area involving the majority of problems. This concept should not lull one into thinking that there are no settlement problems if external indications of settling are not present. There have been cases where failures have occurred in the tank bottom interior plates due to interior settling that did not show any undue settling as monitored by the elevations around the base of the tank.

The threat of settlement failure poses serious consequences to the surrounding property and

safety of life. Until the mid-1950s, tanks were limited to about 200,000-bbl capacity. Since then, the capacity has increased and today 800,000- and 1,000,000-bbl storage tanks are not uncommon. Given the size, it is important that reasonable criteria be available to guide the owner/operator when settling has occurred.

However, the exact mechanisms associated with tank bottom failures due to settlement are complex and seem to defy a rational, all-encompassing design guideline that would prove useful and reliable under all conditions.

Settlement and Failure Mechanisms

Failure effects due to settling can be defined by the occurrence of these effects:

- Floating roof binding within the tank shell
- Damage or early wearing out of floating-roof seals
- Shell buckling in fixed- or floating-roof tanks
- Roof and shell buckling in fixed-roof tanks
- Loss of support of roof support columns in fixed-roof tanks
- Cracking of bottom plate welds
- Loss of acceptable appearance
- Overstress of connected piping
- Accelerated corrosion due to drainage pattern changes outside and under the tank
- Inoperative or less effective water bottoms drainage on the interior of the tank, especially where cone-up or cone-down or single-slope bottoms are used
- Increased susceptibility to seismic damage because of distorted, overstressed, or deformed bottoms
- Leaks in bottom or shells
- Foundation water logging and reduced soil bearing capacities due to inadequate drainage

The most serious failure mode results in leakage or loss of contents. The presence of even a small crack in the tank bottom can pose a serious threat to the integrity of the tank. Several notable settlement failures that have occurred involved the following sequence:

1. Development of an initial leak caused by a crack in the tank bottom.
2. Washout of foundation support immediately near the initial leak location. This causes the crack to grow due to the lack of support, and the leakage increases leading to a vicious cycle of increasing flow.
3. The leak flow increases, and the support under the tank is further undermined to the point where the bottom plates separate from each other or the shell where the foundation has washed away.

Prior to several incidents[1], leakage was seen emanating from under the chime, but the contents

[1] James S. Clarke, *Recent Tank Bottom and Foundation Problems*, Esso Research and Engineering Co., Florham Park, N.J., 1971

could not be pumped out before a major failure occurred.

Basic Settlement Modes

The kinds and modes of settling in tank bottoms are numerous. However, settlement configurations can be more easily dealt with by categorizing them as follows:

- Uniform settlement
- Planar tilt
- Differential shell settlement
- Global dishing
- Local interior settling
- Edge settlement
- Other special cases

We will be primarily discussing uniform settlement, planar tilt, and differential shell settlement.

Uniform settling

In this type of settling, the soil conditions are relatively uniform, and the soil is soft or compressible. A storage tank under these conditions will slowly, but uniformly, sink downward, as shown in Figure 1. In and of itself, there is no significant problem with indefinite uniform settling. However, several important side effects result from this kind of settling:

1. Water intrusion. Water intrusion occurs when a depression or water trap is formed around the external periphery of the tank where it meets the soil. When it rains or floods, moisture accumulates under the tank bottom near the shell or chime region and acts to corrode the bottom. Also, any moisture under the tank may condense, may be unable to escape to the atmosphere, and may be trapped under the shell, causing corrosion.
2. Piping. Piping connected to the tank or piping supports too close to the tank will eventually become overstressed by the movement of the tank relative to the piping and its supports. This is sometimes called *over-constrained piping*.
3. Inability of pooling hydrocarbons around the perimeter of the tank pose a serious fire threat.

It is possible to assess the degree of uniform settlement by simply monitoring elevations at the base of the tank on the chime.

DRAFT

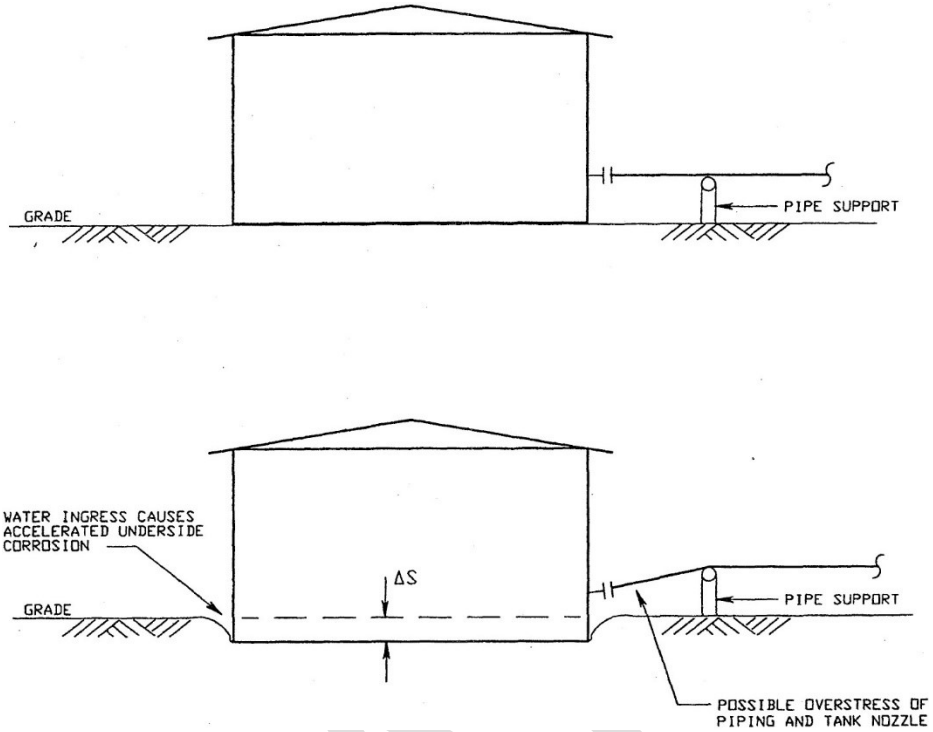

Figure 1. Rigid Settlement without Tilt

Planar tilt

This is a more general rigid body translation than uniform settlement where tilting occurs along with uniform settlement. In this mode, the tank settles vertically and rotates or tips as a rigid structure (see Figure 2). As shown in Figure 3, the elevation at the bottom of the shell follows a cosine-wave as a function of angular distance from the high point. In API 653, this representation of planar tilt is referred to as the "cosine curve". To see this, assume the high and low points are on the x-axis and that the tank settled by pivoting on the y-axis.

Prior to settlement, the bottom edge of the shell was a circle in the x-y plane,

$$\begin{pmatrix} x \\ y \\ z \end{pmatrix} = \begin{pmatrix} R \cdot \cos(\alpha) \\ R \cdot \sin(\alpha) \\ 0 \end{pmatrix}$$

where R is the radius and α is the clockwise angle from the y axis. Assuming that the tank settled an average of s feet while rigidly pivoting δ radians around the y axis, the bottom edge of the shell becomes a circle on the tilt-plane (see Figure 4). Its new coordinates are:

$$\begin{pmatrix} X \\ Y \\ Z \end{pmatrix} = \begin{bmatrix} \cos(\delta) & 0 & -\sin(\delta) \\ 0 & 1 & 0 \\ \sin(\delta) & 0 & \cos(\delta) \end{bmatrix} \begin{pmatrix} x \\ y \\ z \end{pmatrix} - \begin{pmatrix} 0 \\ 0 \\ s \end{pmatrix}$$

$$(new\,coordinates) = [rotation] \times (old\ coordinates) - (translation)$$

The bottom edge of the shell is now a circle on the tilt-plane

$$\begin{pmatrix} X \\ Y \\ Z \end{pmatrix} = \begin{pmatrix} x \cdot \cos(\delta) \\ y \\ x \cdot \sin(\delta) - s \end{pmatrix} \tag{1}$$

the depth of settlement (Z) is now a sine wave with amplitude $R \cdot \sin(\delta)$,

$$Z = R \cdot \sin(\delta) \cdot \sin(\alpha) - s = A \cdot \sin(\alpha) - s\,, \tag{2}$$

and the plan view is an ellipse

$$\begin{pmatrix} X \\ Y \end{pmatrix} = \begin{pmatrix} x \cdot \cos(\delta) \\ y \end{pmatrix} = \begin{pmatrix} R \cdot \cos(\alpha) \cdot \cos(\delta) \\ R \cdot \sin(\alpha) \end{pmatrix}$$

When the pivot line is not aligned with the y axis there will also be a phase angle,

$$Z = A \cdot \sin(\alpha - \varphi) - s = A \cdot \cos(\alpha - \varphi - \pi/2)\,.$$

A statistically significant, one-cycle cosine component of settlement depth is the signature of rigid-body tilt. This component produces no bending stresses in the tank shell and should always be removed from the settlement data.

DRAFT

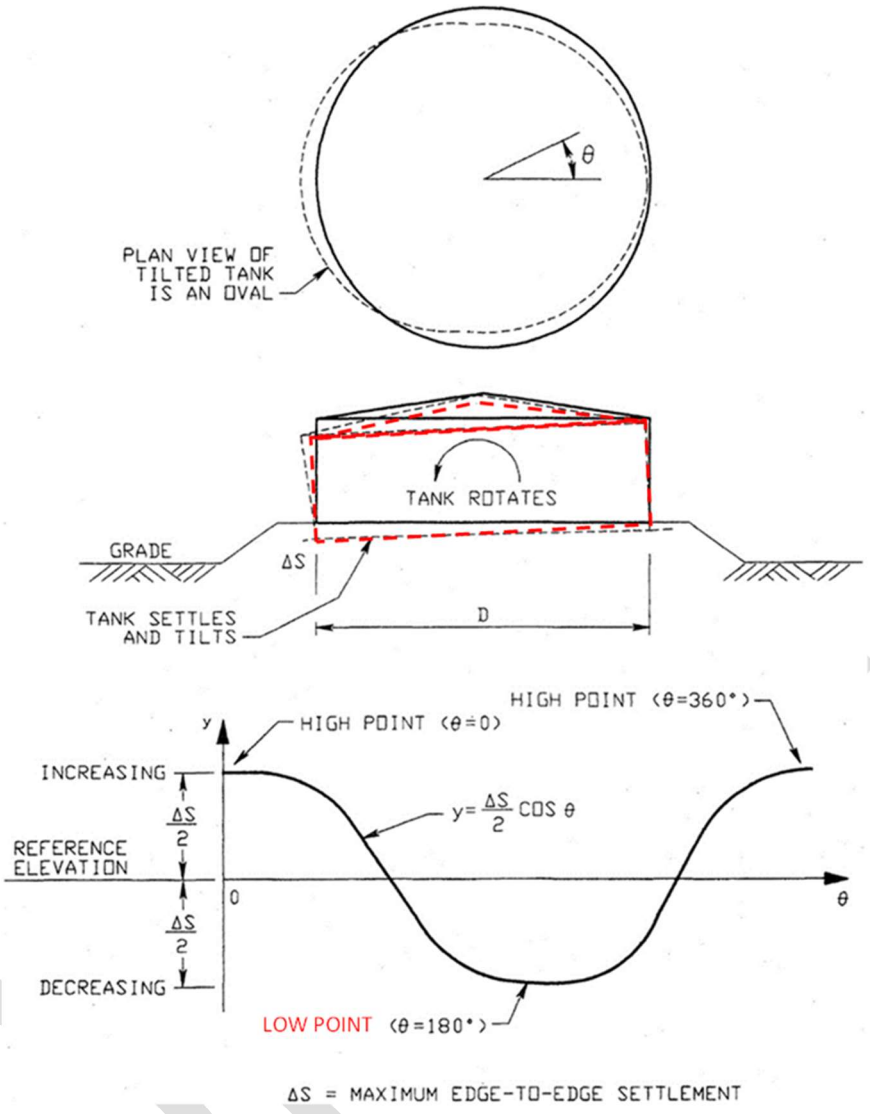

Figure 2. Settlement with Rigid Tilt

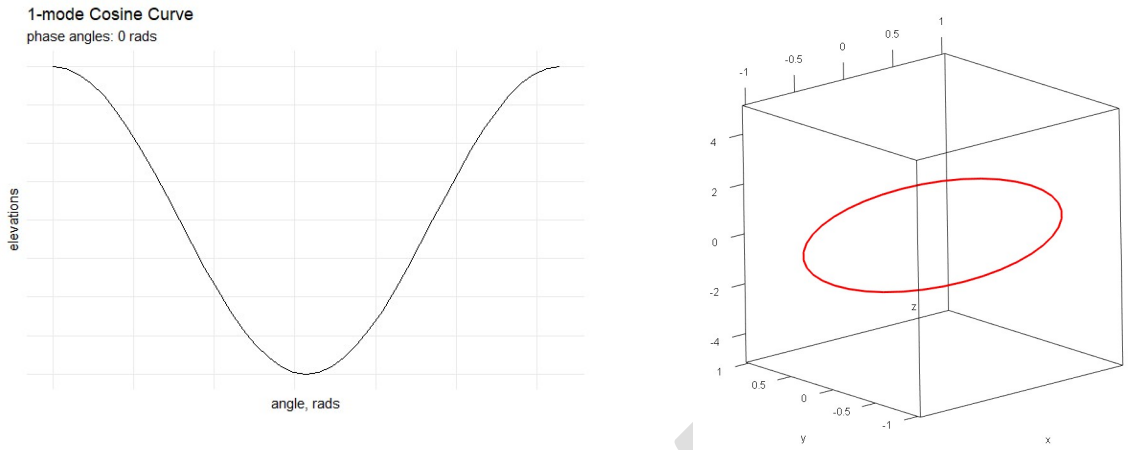

Figure 3. An example of how a cosine curve looks like a tilted circle in 3D.

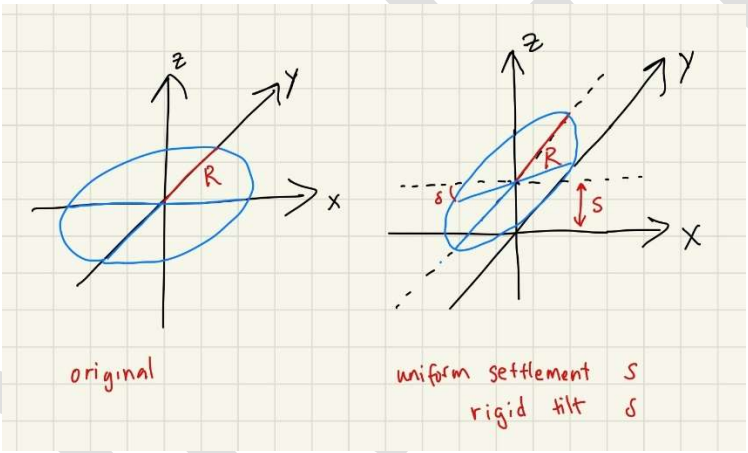

Figure 4. Translation s in the Z-axis with rotation δ about the y-axis.

How to Estimate Rigid Tilt from Settlement Data

In Figure 6 we show how to use Excel's regression tool[2] to estimate the tilt plane. The data are settlement measures (Z) taken at 16 evenly spaced stations along the base of the shell with respect to an arbitrary reference elevation or benchmark. The diameter of the tank is 120 feet, so the circumference is π×120 = 377 feet and the spacing between stations is 377/16 = 23.56 feet. Column "theta" is the number of radians from station 1; theta = 2×π×(Station-1)/16. "cos" and "sin" are the cosines and sines of theta. We instructed Excel to regress settlement on cosine and sine. The result is,

[2] PEMY Consulting provides an example calculation on github at the URL https://github.com/rbitip/settlement-excel-regression-too

$$\hat{z} = -1.147 - 0.337 \cdot \cos(\theta) - 0.408 \cdot \sin(\theta)$$

We convert this to cosine with phase angle form by using the trigonometric identity,

$$a \cdot \cos(t) + b \cdot \sin(t) = A \cdot \cos(t - \varphi),$$

where amplitude $A = \text{sgn}(a) \cdot \sqrt{a^2 + b^2} = -0.526$, and phase angle $\varphi = \arctan(b/a) = 0.889$. So, the z-value of the cosine model of the tilted plane is,

$$\hat{z} = -1.147 - 0.526 \cdot \cos(\theta - 0.889) = M + A \cdot \cos(\theta - \varphi), \quad (3)$$

where M is mean settlement, $\pm A$ is the range, $|A|$ is the amplitude of settlement, and φ is the phase angle from the first measurement station (where arc length is zero). Deviations of observed values (z) from fitted values ($\hat{z}$) are called "residuals. In settlement analysis, residuals from the tilted plane are called "out of plane deflections". The symbol for an out of plane deflection is U. Figure 5 (left panel) is a graph of raw settlement data values (Z) and the tilted plane that best fits the data ($\hat{z}$, the dashed red line). The right panel shows out of plane deflections. The out of plane deflection for the 9th observation is shown in both panels.

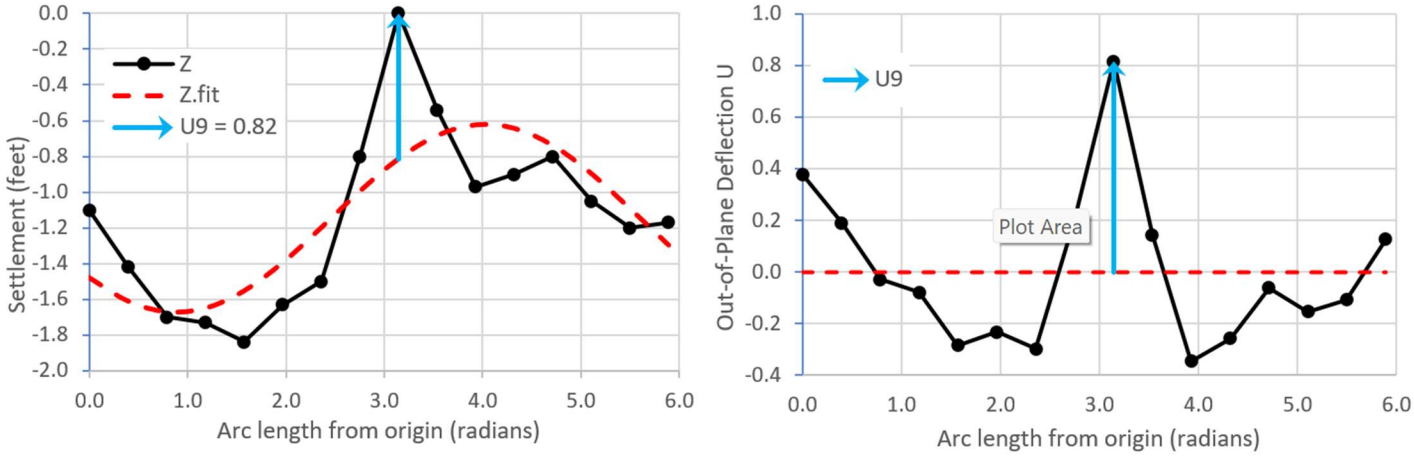

Figure 5. Left: Excel plot of Settlement and Tilted Plane. Right: Residual Deviations from Plane

Adjusted R^2 and p value

Adjusted R^2 (coefficient of determination) is a measure of how much of the total variance is accounted for by the tilted plane. In this case the tilted plane is responsible. The tilt-plane analysis in Figure 5 had adj R^2 = 0.558, meaning that the sinusoidal variation of the tilt plane around the bottom of the tank accounted for 55.8% of the change of elevation of measured settlement. Adjusted R^2 is not a test for whether the tilt plane belongs in the analysis, that is the job of the *p*-value. For the case of the tilt-plane analysis in Figure 5, the p-value was 0.002. This p-value indicates that the tilt plane is highly statistically significant. Conventionally p-values below 0.05 are considered statistically significant. However, in the case of a control variable, like planar tilt, it is customary to retain that term if the p-value is less than 0.15.

Tank Data		Computed Values (do not enter)					Regression on cos and sin.					
Station	Z[a]	theta	cos	sin	Z.fit[b]	U[c]	*Regression Stats*		Computed Parameters			
1	-1.10	0.000	1.00	0.00	-1.48	0.38	Adj R Sqr	0.558	Amplitude	-0.526		
2	-1.42	0.393	0.92	0.38	-1.61	0.19	Resid se	0.325	Phase	0.888		
3	-1.70	0.785	0.71	0.71	-1.67	-0.03	n	16				
4	-1.73	1.178	0.38	0.92	-1.65	-0.08	Analysis of Variance Table					
5	-1.84	1.571	0.00	1.00	-1.56	-0.28	*Source*	*df*	*SS*	*MS*	*F*	*p-val*
6	-1.63	1.963	-0.38	0.92	-1.40	-0.23	Tilt	2	2.214	1.107	10.46	**0.002**
7	-1.50	2.356	-0.71	0.71	-1.20	-0.30	Residual	13	1.376	0.106		
8	-0.80	2.749	-0.92	0.38	-1.00	0.20	Regression Coefficients					
9	0.00	3.142	-1.00	0.00	-0.82	0.82		Est	se	p-val	95% Conf. Int.	
10	-0.54	3.534	-0.92	-0.38	-0.68	0.14	Intercept	-1.147	0.081	0.000	-1.32	-0.97
11	-0.97	3.927	-0.71	-0.71	-0.62	-0.35	cos(theta)	-0.332	0.115	0.006	-0.58	-0.08
12	-0.90	4.320	-0.38	-0.92	-0.64	-0.26	sin(theta)	-0.408	0.115	0.002	-0.66	-0.16
13	-0.80	4.712	0.00	-1.00	-0.74	-0.06	**Definitions**					
14	-1.05	5.105	0.38	-0.92	-0.90	-0.15	a) Z: elevation of tank bottom relative to datum					
15	-1.20	5.498	0.71	-0.71	-1.09	-0.11	b) Z.fit: best-fit tilt plane					
16	-1.17	5.890	0.92	-0.38	-1.30	0.13	c) U = (Z – Z.fit): out-of-plane deflection					

Figure 6. Planar tilt for Andreani's[3] example 2. The complement of the *p*-value, 1-p = 0.998, is the analyst's *confidence*[4] in saying "the tilt angle is not zero."

Consequences of Planar Tilt

Typically, planar tilt accompanies uniform settlement. In addition to the concerns addressed for uniform settling there are several additional phenomena that occur as the tilt becomes severe.

Appearance

The human eye is sensitive to horizontal and vertical lines. With a relatively small angle of tilt, the tank begins to look strange. This can cause the public, employees, or anyone else to begin to question the safety of the tank and the operating and maintenance practices of the owner/operator. Planar tilt limited to 1/50th of tank diameter (D) is a reasonable plumbness

[3] Andreani, J.L., and Carr, N.A. *Study of Out-of-Plane Tank Settlement*, API, Washington, D.C., May 2007. The data in Figure 6 (Andreani et al.'s Example 2) are 16 equally-spaced settlement measurements around the perimeter of a 120 x 40 foot (Diameter x Height) floating roof tank.

[4] Confidence and its Bayesian analogue, *credibility*, are complicated topics. Saying "I am 99.8% confident that the bottom is tilted," means, "if there were no real tilt, then there is only 0.2% probability that the estimated tilt will be this big."

specification that provides an acceptable tank appearance.

Note that API 650 limits new tank construction plumbness to 1/200. API 653 limits the total plumbness to 1/100 for reconstructed tanks with a limit of 5 in. maximum. These are both well within the visually noticeable limits of 1/50.

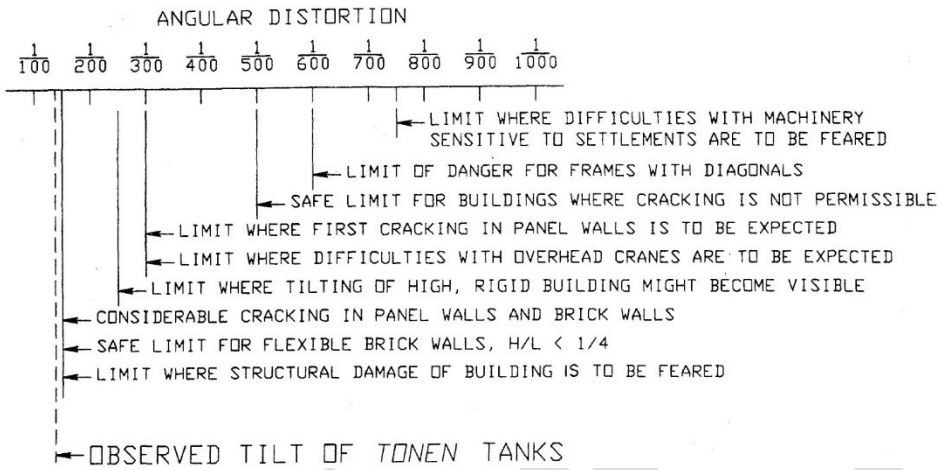

Figure 7. The effects of increasing angular distortion.

Hydrostatic Increase

The tilt of the tank results in a slight increase of the hydrostatic head for a given liquid volume. The increase in hydrostatic head may be estimated approximately by $D \cdot \Delta S/2$, where *D* is the tank diameter and ΔS is the high-to-low difference in tank bottom elevation. While there is a slight increase the shell stresses this is usually not a cause for concern.

Assessment of Planar Tilt

The assessment process for planar tilt is similar to the process for uniform settlement. The external connections which are not flexible (i.e., piping, stairs rigidly connected to grade or other fixed points not attached to the tank) will shift as the tank settles, causing high forces as the tank moves relative to the fixed points. Planar tilt can be assessed from an external tank inspection conducted by taking elevation readings at several locations around the base of the tank.

Storage capacity reduced. If the tank is filled to the maximum working level, the tilt can result in a negligible reduction of the working capacity. This would only be true for operators who run the normal working level up to some physical limit such as an overflow in some cases (which is not considered good practice).

Like uniform settlement, planar tilt does not really have much effect on the tank structure other than attachments such as stairway landings or piping that is attached to the tank. Planar tilt does not cause stress; stress comes from curvature which shows up as out-of-plane deflections. The apparent sinusoidal curvature of the tilted plane is an artifact of the frame of reference (like the apparent daily "motion" of the sun moving up and down in the sky). Later in this chapter, when discussing API 653 methods for evaluating out-of-plane differential settlement, it will be clear

that the effect of planar tilt *must be removed* from settlement data to correctly understand the true strain at the bottom of the tank shell.

Although limits on the amount of planar tilt have been proposed, there is not enough stress or changes in the tank or liquid geometry to be a cause for concern. In extreme cases of planar tilt, the first noticeable problem is its visual impact (it is for this reason that the Leaning Tower of Pisa is so famous). If employees or the public see a tank which is visibly tilted, they naturally become concerned about the tank's integrity itself or question the integrity of operations and its management.

Cosine Curves of Higher Modes

While API 653 only addresses 1-mode cosine curves (planar tilt), we have observed that tanks commonly settle differentially into 2-modes and 3-modes. A single fold across or near the diameter results in 2-mode folding, resulting in the disk of the tank bottom folding into a "taco" configuration. In 3-mode folding there are 2 folds, resulting in a "lawn chair" configuration. As shown in Figure 8, the appearance of the cosine curve changes as the phase angle changes.

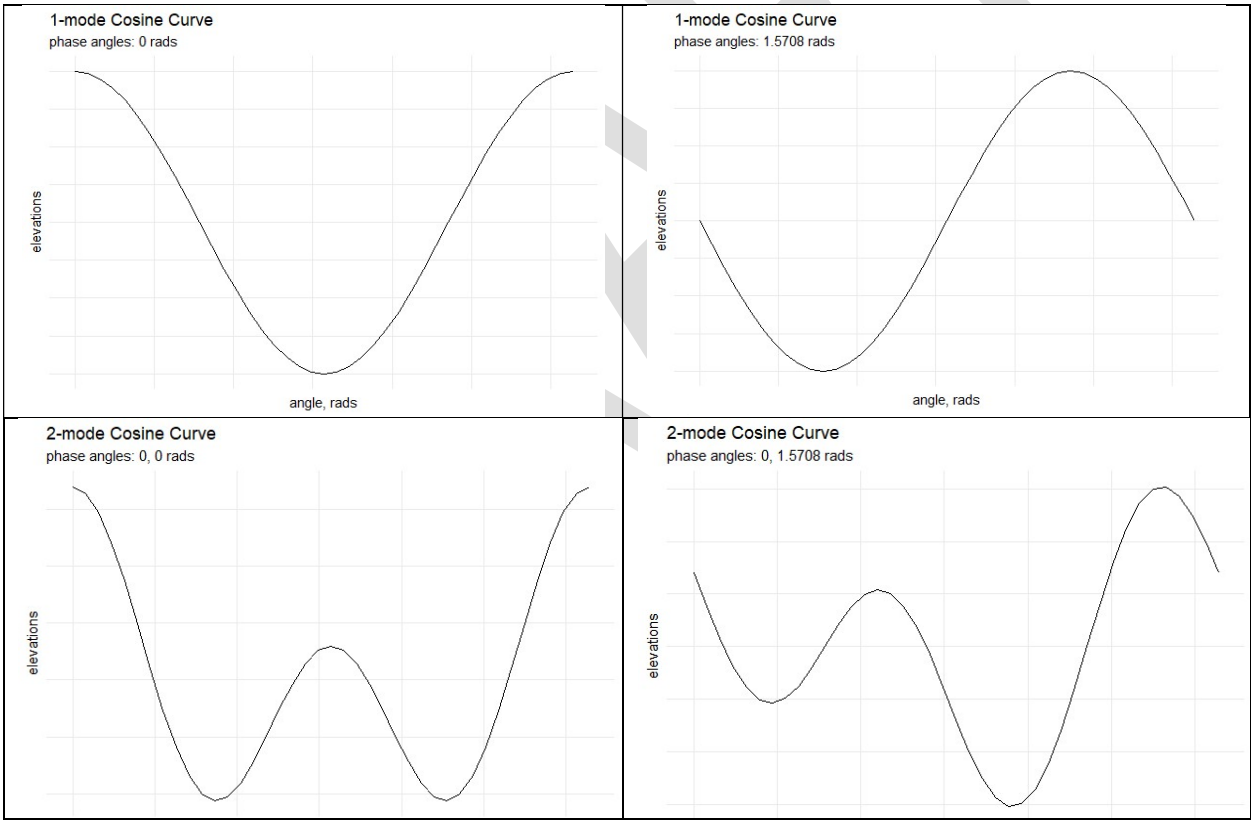

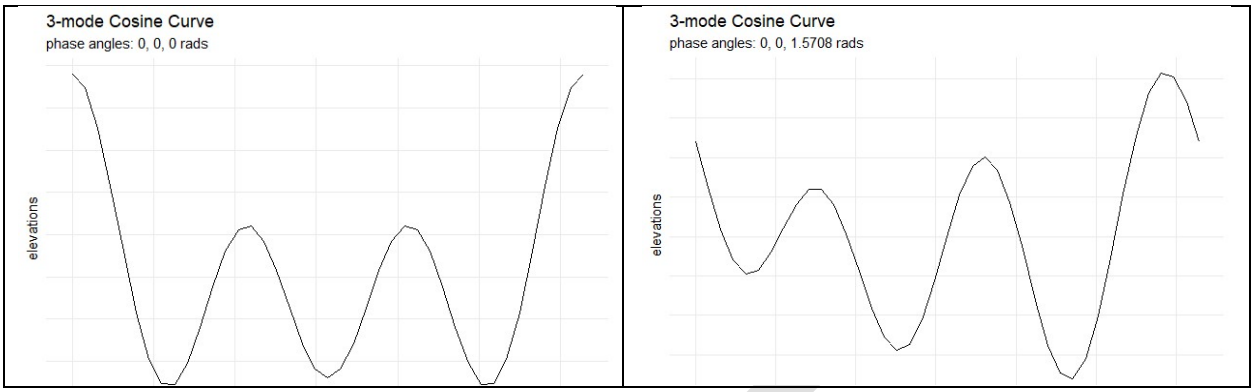

Figure 8. From top to bottom, curves increase in number of modes from 1 to 2 to 3. Curves on the left have phase angle set to 0; Curves on the right have their highest frequency mode shifted 90 degrees to the right (+1.5708 radians).

Real world settlement data provides some insight as to the use of higher-mode cosine curves. Consider Figure 9 and Figure 10.

One measure of the "goodness" of a curve fit is the adjusted R^2 value, discussed before. To put it simply, it quantifies how closely the fit matches the data points. API 653 considers a cosine curve fit valid if it meets certain R^2 criteria. Later on, in the section titled *The tilt plane should always be subtracted from raw settlement values*, we discuss how an R^2 value minimum threshold is not the "end all be all" for determining whether a fit is appropriate to use. However, we will note that, given the choice between two models, a higher adjusted R^2 is preferred if adding a higher mode to a model reduces adjusted R^2, that mode should not be in the model.

P-values are discussed in more depth later as well – in summary, a lower p-value means there is evidence that a mode should be in the model to properly represent the data. Traditionally, *p*-values should be below 0.05 or even 0.01 for confirming possible causal factors (as in a drug trial), but can be up to 0.15 for fitting data to smooth noisy data, as in a settlement analysis. Leaving out a term with low p-value would result in an inadequate model.

For Figure 9, regular cosine fit has an adjusted R^2 value of only 0.15. In comparison, Figure 10 uses a 2-mode cosine fit where a single fold is considered. This makes a superior fit, with adjusted $R^2 = 0.99$. This is a significant improvement in R^2 which, as noted before, indicates that the 2-mode cosine is a better fit. In addition, the use of a 2-mode cosine has a substantially lower p-value than the 1-mode cosine, which is a meaningful improvement.

API 653 only uses single mode cosines curves and would reject the 2-mode cosine regression curve for the given settlement data. This does not seem reasonable. The tank does not have issues with high stresses induced in the bottom or the corner joint of the shell to bottom because of the low curvature. Rather, the fold acts to produce out of roundness near the top of the tank as well as upper course high shell stresses. In this case, the focus of engineering should be the impact of out of roundness and effects on the seals and the potential for buckling, not on the bottom.

DRAFT

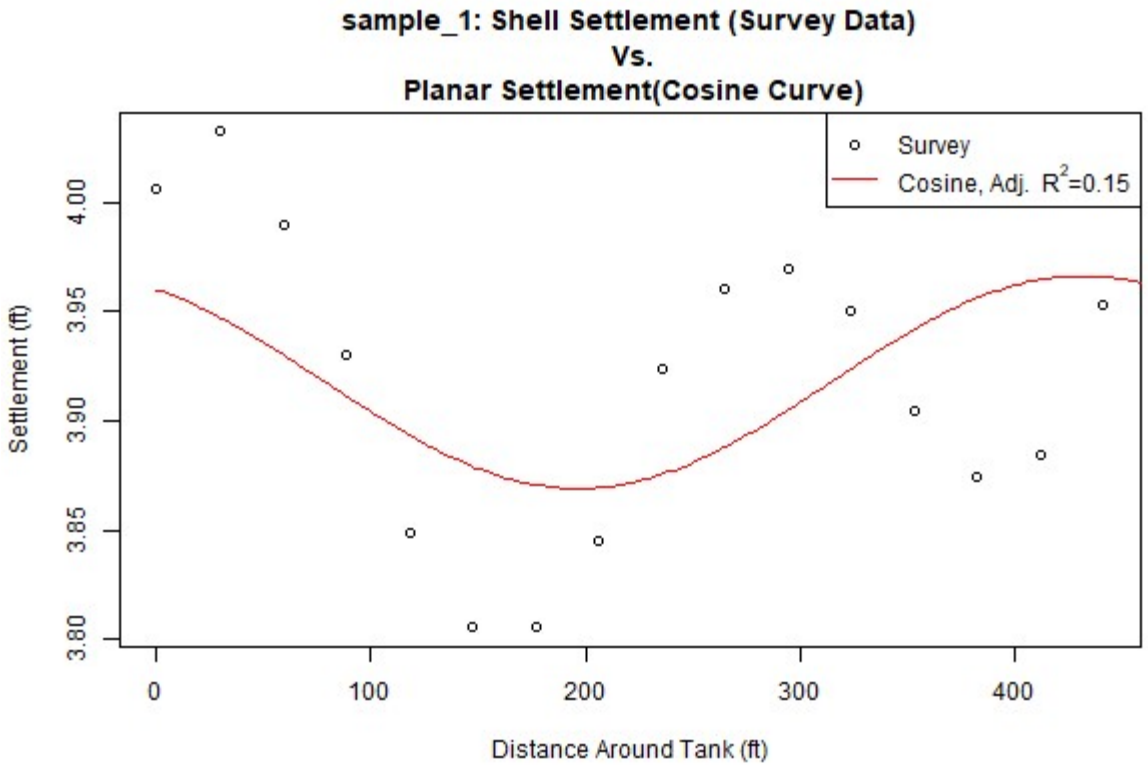

Figure 9. A 1-mode cosine fit to settlement data. It could be improved…

DRAFT

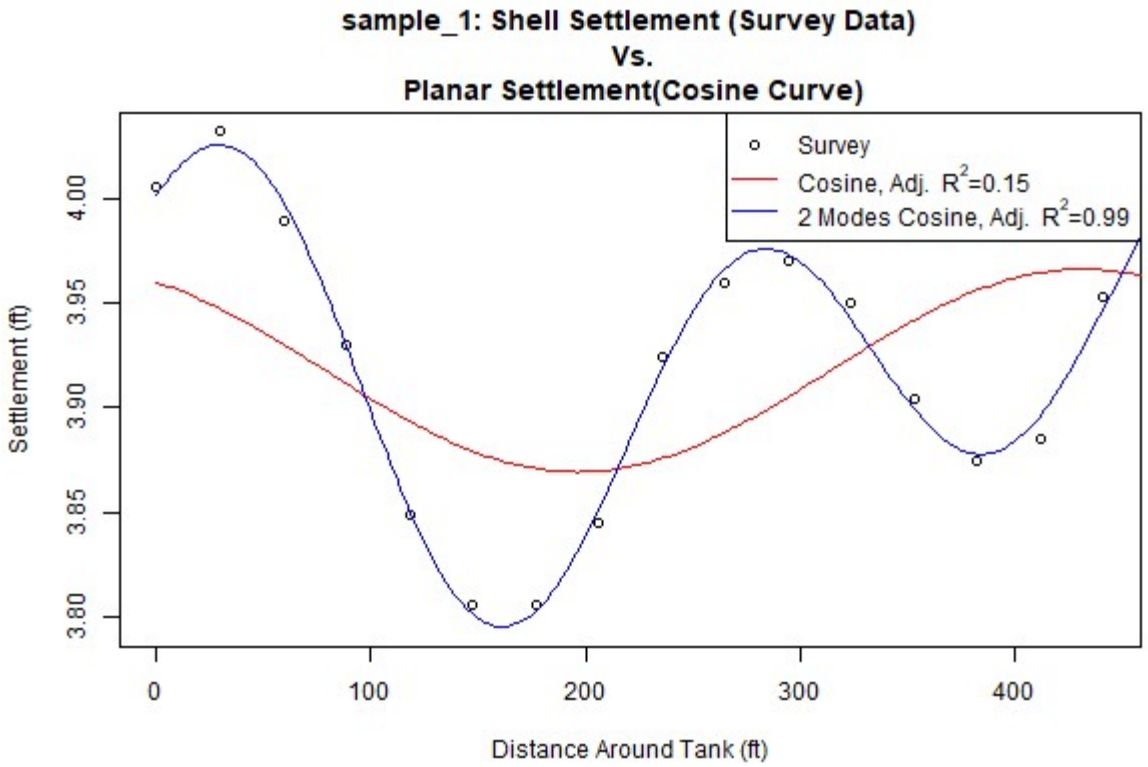

Figure 10. A 2-mode cosine fit to settlement data. An improvement over the 1-mode fit.

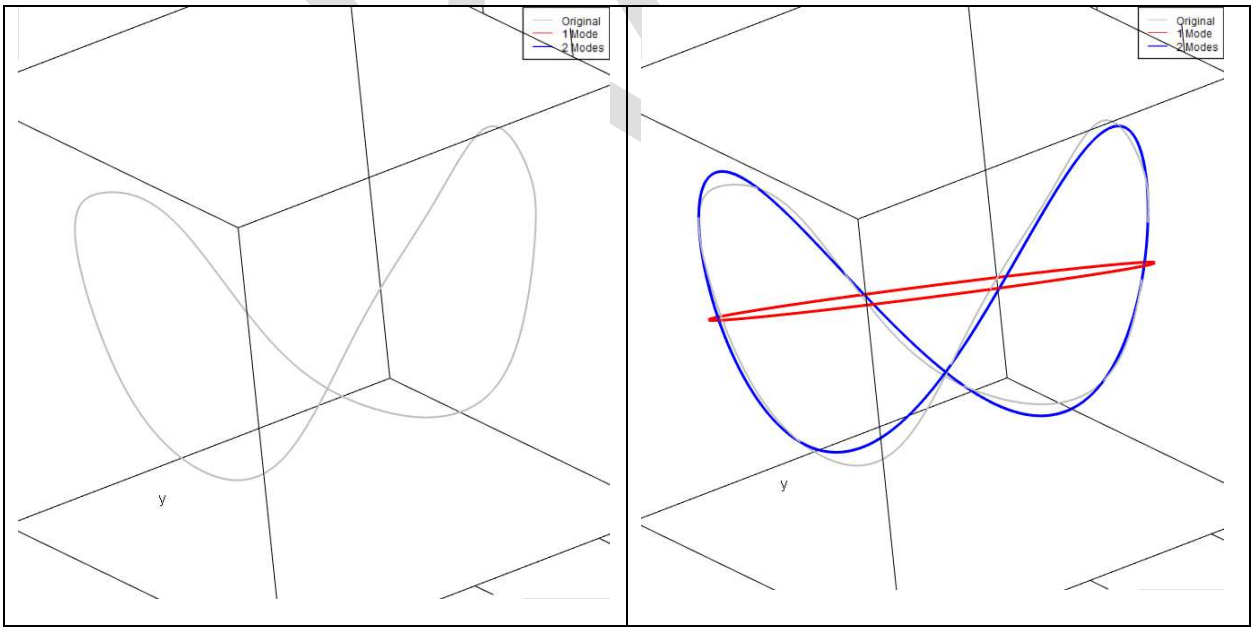

Figure 11. Left: the settlement data used in Figure 9 and Figure 10 shown in 3D.
Right: the 1-mode (in red) and 2-mode (in blue) cosine fit shown in 3D.

Cosine curves of 3-modes. There are situations where a 2-mode cosine fit can be either unnecessary or insufficient. For example, in Figure 12, changing from a one-mode to two-mode cosine fit does not yield significant improvement in its adjusted R^2. In contrast, the 3-mode cosine yields a significant improvement in adjusted R^2 and fits the best for this settlement data.

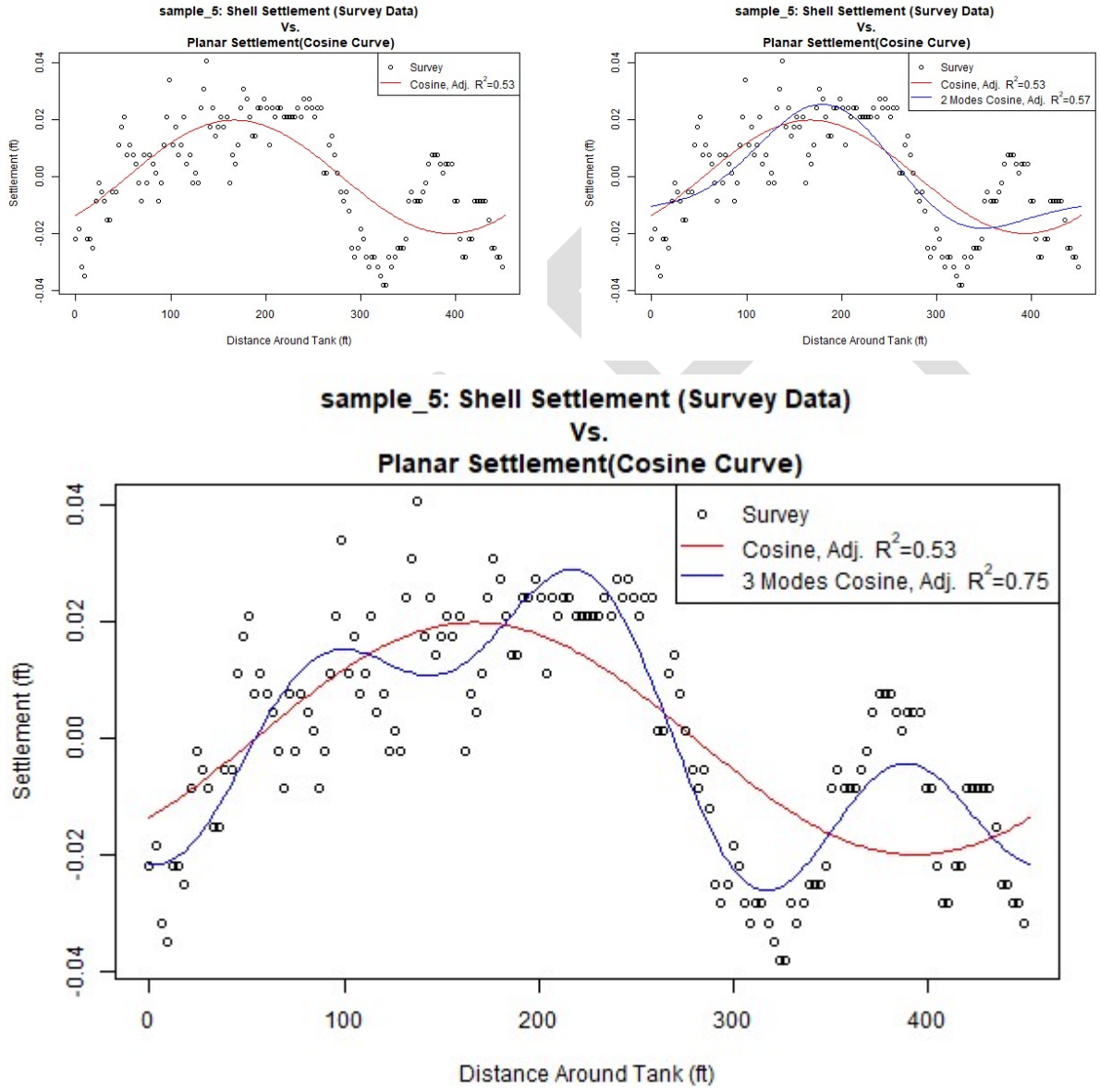

Figure 12. The 3-mode cosine fits the best for this settlement data.

 Copyright PEMY Consulting, LLC

API 653 Differential Settlement Analysis

Differential settlement involves deflections from a tilted settlement plane. Unlike rigid settlement and tilt, these deflections do cause bending strain in the tank shell that may lead to distortions, cracking, and possibly leakage.

The current authoritative resource for large flat bottom tank differential settlement is API 653 Annex B "Evaluation of Tank Bottom Settlement". Differential settlement may be local and global bulges and dishing, or settlement near the shell that deviates from the cosine curve as in Figure 13. Many researchers have contributed to the settlement criteria used today. While local and global bulges and dishing can be analyzed by simplified models such as those given in stress analysis textbooks, differential settlement has defied even approximate solutions until recently. API 653 Annex B offers two of those approximate methods. However, these are only screening methods that identify possible areas of excess stress needing follow-up. Ultimately, finite element analysis is considered the gold standard.

Overview of API 653 Methods

API 653's differential settlement analysis methods follow a procedure, like so:

1. For given settlement data, calculate the regular 1-mode cosine curve fit. This cosine curve fit is a combined approximation of the uniform settlement and planar tilt, without out-of-plane bottom distortion.
2. The out-of-plane settlement U, measured in in the same units as tank circumference (either feet or meters) is calculated by subtracting the cosine curve fit from the settlement data
   ($U_i = Z_i - \hat{z}_i$, where *Z* is the observed settlement data (feet), $\hat{z}$ is the cosine curve fit, and the subscript *i* denotes these are their values for data point *i*).
3. The out-of-plane settlement is used to approximate the out-of-plane deflections S.
4. The out-of-plane deflections are compared against the maximum permissible settlement S_{max}.

API 653 5th Edition, Annex B, describes two methods for analyzing the resulting out-of-plane settlement and determining whether the settlement data profile is within allowable bounds. Annex B also describes a third method that does not utilize the cosine curve fit – for reasons described later, we do not recommend the use of this method.

The first of these two methods we call Marr et al's method, or Marr's method. It is the default method of analysis in API 653 B.2.2.4. In this method, the out-of-plane settlement (U_i for data point *i*) is used to calculate the out-of-plane deflection (S_i). As described in API 653 figure B.3, the out-of-deflection for point *i* is

$$S_i = U_i - \left(\frac{1}{2} U_{i-1} + \frac{1}{2} U_{i+1} \right) \tag{4}$$

The maximum permissible settlement for Marr's method, per API 653 B.3.2.1, is

$$S_{max} = \frac{11 \cdot (L^2 \cdot Y)}{2 \cdot (E \cdot H)} \tag{5}$$

Where,

L is arc length between (evenly spaced) measurement points, in feet,

Y is the yield strength of the shell material,

E is Young's Modulus of the shell material, and

H is the tank height, in feet (ft).

The second of these two methods we call Andreani's method. This method is applicable if the tank's out-of-plane deflections exceed the maximum permissible settlement by Marr's method, per API 653 B.2.2.5.2. For this method, the out-of-plane settlement is directly compared with the maximum permissible settlement (API 653 B.5). That is, $U_i = S_i$. The maximum permissible settlement for Andreani's method is, per API 653 B.3.2.2,

$$S_{max} = \min \left(K \cdot S_{arc} \frac{D}{H} \frac{Y}{E}, 4.0\,in \right) \tag{6}$$

Where,

K is a tabulated value from Table 1, calculated empirically from FEA results that depends on diameter and type of roof,

$S_{arc,i} = L_i$ = settlement arc length, ft = distance between the two zeroes that define the arc.

D = tank diameter, ft

H = tank height, ft

Y = yield strength, psi

E = Young's Modulus, psi

DRAFT

Tank Diameter ft	K, Open Top Tanks	K, Fixed Roof Tanks
$D \leq 50$	28.7	10.5
$50 < D \leq 80$	7.8	5.8
$80 < D \leq 120$	6.5	3.9
$120 < D \leq 180$	4.0	2.3
$180 < D \leq 240$	3.6	Not applicable
$240 < D \leq 300$	2.4	Not applicable
$300 < D$	Not applicable	Not applicable

Table 1. API 653 K* table from Section B.3.2.2

These two methods will be explored in greater detail in the following sections. We later comment on the 3rd API 653 method, which we do not recommended.

Marr's Method

For differential settlement, API felt in the 1990s that there was sufficient research to put limiting rules into API 653 to cover differential settlement. The first rule is based on the paper by Marr et al[5]. Marr summarized previous work going back to at least the 1960s and provided data and analyses for settlement criteria for tanks at Kawasaki, Japan. Marr reviewed the criteria suggested by the most important tank settlement work. They covered work on planar, non-planar (i.e., differential), ovality, and local settlement modes. Marr and his co-authors concluded that the work of Malik (1977), based on beam theory, best addressed differential settlement.

Their proposal has been incorporated and still exists in API 653[6] as appendix section B.2.2.4 It is based on out of plane deflections from the plane of rigid tilt that has the least RMS deviation[7] from the data. Deflections, labeled $U_1, U_2, \cdots, U_n$ in Figure 13, are observed settlement values minus the cosine representation of the tilt plane,

$$U_i = Z_i - \hat{z}_i = Z_i - \left(M + A \cdot \cos\left(\theta_i - \varphi\right)\right) \tag{7}$$

[5] W. A. Marr, J. A. Ramos, and T. W. Lambe, "Criteria for Settlement of Tanks," *Journal of Geotechnical Engineering*, 108(GT8), August 1982.

[6] API Standard 653, 5th Ed., Nov. 2014, Addendum 2, May. 2020

[7] Root-Mean-Square deviation; the square root of the average squared deviation (*standard deviation*, or standard error).

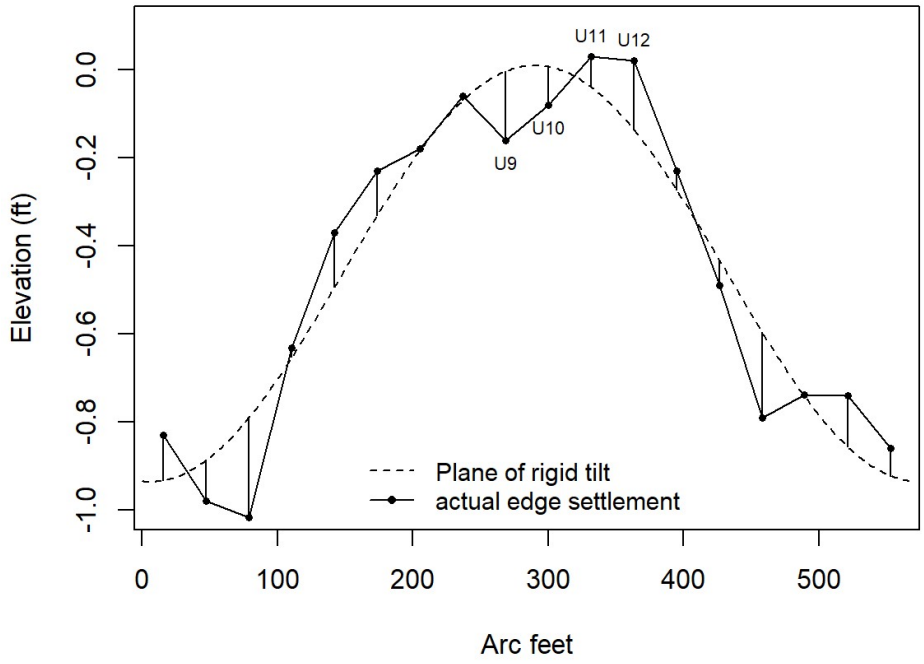

Figure 13. Deflections (U) from plane of rigid tilt.

The tilt plane should *always* be subtracted from raw settlement values

In saying this, we directly contradict the advice in API 653, paragraph B.2.2.4:

> *In many cases, the out-of-plane settlement may be concentrated in one or more areas. In such cases, the least-squares fit approach may under predict the local out-of-plane settlement and is not conservative. In these cases, R^2 will typically be less than 0.9, and more rigorous curve-fitting procedures should be considered. Alternatively, the settlement may not indicate a well-defined rigid tilt plane and the procedure in B.2.2.5 should be considered…*

This suggestion is *wrong* and should be ignored. It comes from a misunderstanding of the statistic R^2, a number in the interval [0,1] described as "the proportion of variance explained by the (planar tilt) model". The misunderstanding is the claim that a model is not valid unless R^2 is very high, say 0.9 or above. This is simply not true for several reasons. First, R^2 is incorrect; the correct criterion is adjusted R^2. Second, no model can account for pure noise. Third, candidate exploratory variables are selected solely for their ability to *increase* adjusted R^2. Large R^2 is not required and may be impossible due to measurement noise.

When there is a list of potential explanatory variables (e.g., cosines and sines with frequencies equal to or greater than 1), standard practice is to find the set of variables that together produce the highest attainable adjusted R^2. This is called variable selection. The simplest way to do this is forward stepwise regression, which starts with an intercept only and successively incorporates the remaining unincorporated variable that produces the largest *increase* in adjusted R-

squared. It stops when none of the remaining variables increases the value of adjusted R^2. In other words, keep adding variables that predict better than chance. A common variant is to keep adding variables as long as they *significantly*[8] increase adjusted R^2.

We saw in Figure 6 that the variables defining planar tilt, cos(theta) and sin(theta), are individually and jointly significant. Here, the word *significant*, means, roughly, "it is highly likely that the settlement of this tank has a tilt component".

Subtracting the tilt plane is analogous to subtracting the mean when computing a standard deviation. The tilt plane is incapable of introducing bias in out-of-plane deflections and leaving it out unnecessarily complicates the statistical analysis of out-of-plane deflections.

Conclusion: Always compute the tilt plane and subtract it from the depth measurements.

Marr's criterion for excess out-of-plane deflections.

The data model for out-of-plane deflections is,

$$U_i = u(\ell_i) + e_i, \tag{8}$$

where e is noise, a combination of roughness[9] and measurement error, ℓ_i is the arc length in feet between the first and ith measurement station, and $u(\ell)$ is the true deflection value at arc length ℓ. Figure 14 shows the relationship between observed deflections and a hypothetical true deflection curve.

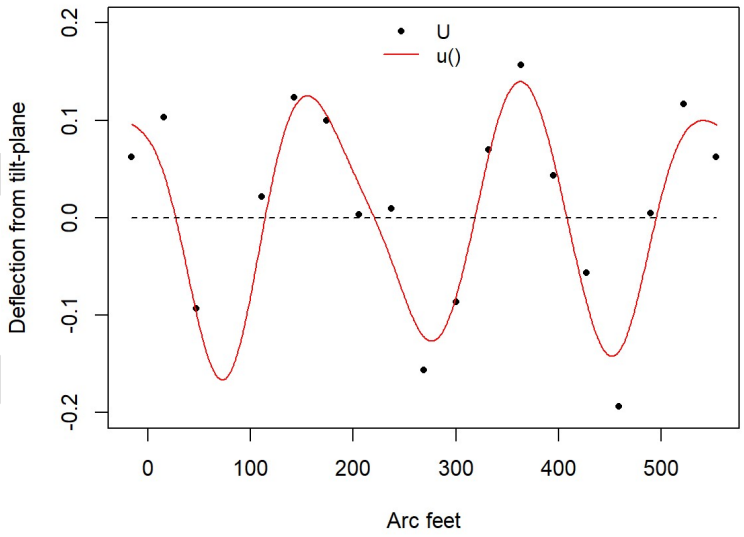

[8] Statistical significance is determined by the *p*-value. When building a regression model, *p*-values smaller than 0.10 are considered significant.

[9] Roughness includes all deviations from smoothness that are not due to settlement and are not measurement errors (overlapping plates, welds, etc.)

Figure 14. Deflections, U, from tilt plane and a hypothetical true deflection curve, $u(\ell)$.

Beam Theory

Marr et al.[5] developed the first API 653 settlement analysis procedure (API 653 appendix B.2.2.4), based on Euler Bernoulli beam theory (EBBT), treating the tank shell as a beam. The "beam" is, conceptually, the result of slitting the tank shell from top to bottom, separating it from the tank bottom, and unrolling it, as in Figure 15.

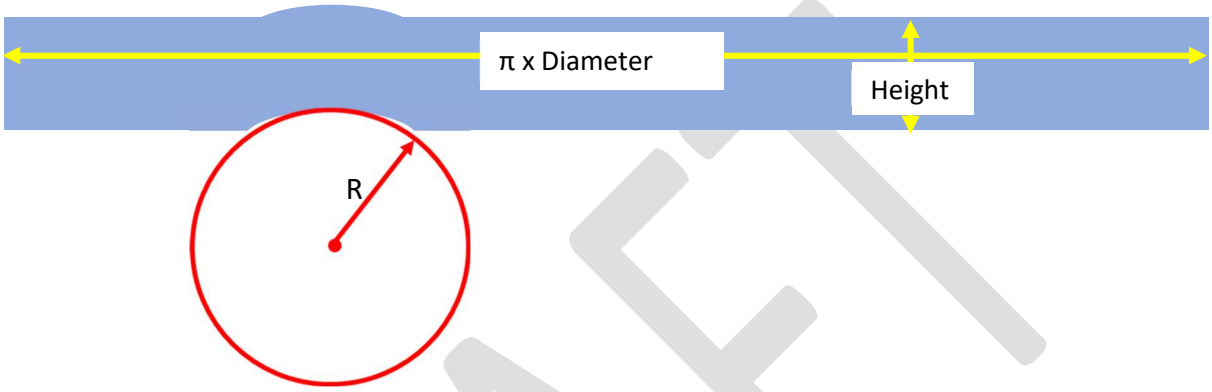

Figure 15. Unrolled tank bottom showing Radius of curvature[10] of an out-of-plane deflection.

The problem with EBBT is that it assumes that the beam cannot flex laterally to relieve stress, e.g., by dimpling, buckling, and ovalizing.

In Euler-Bernoulli beam theory, bending strain, ε, of a beam at a distance y above or below the neutral axis of the beam is $\varepsilon = y/R = \kappa \cdot y$, where *R* is the radius of curvature of an out of plane deflection. The reciprocal, $\kappa = 1/R$, is the curvature.

Since stress, σ, is proportional to strain,

$$\sigma = \kappa \cdot E \cdot y \tag{9}$$

where *E* is Young's modulus for the shell material.

The neutral axis is at the geometric center of the beam cross-section. In theory, there is no strain at the neutral axis and therefore its length does not change under bending. API 653 appears to assume the neutral axis is at half the height of the tank, which would be correct for a rectangular beam. However, tank walls can taper from 1/4" at the top to 7/8" at the bottom. In addition, the

[10] The radius of curvature at a point on a deflection arc is the radius of the *osculating* circle that touches the deflection arc and has the same first and second derivatives as the arc at the point of contact. This definition assumes the same units (feet, meters) on the horizontal and vertical axes.

tank top and bottom have differing amounts of stiffening, such as when the shell is welded to an annular ring which might be 7/8" thick by 30" wide.

Marr's Empirical Bound on Top of Shell Tensile Stress

Marr, et al.[5] estimated curvature at each measurement station using three adjacent out-of-plane deflection measurements, U_1, U_2, U_3 as shown in Figure 16.

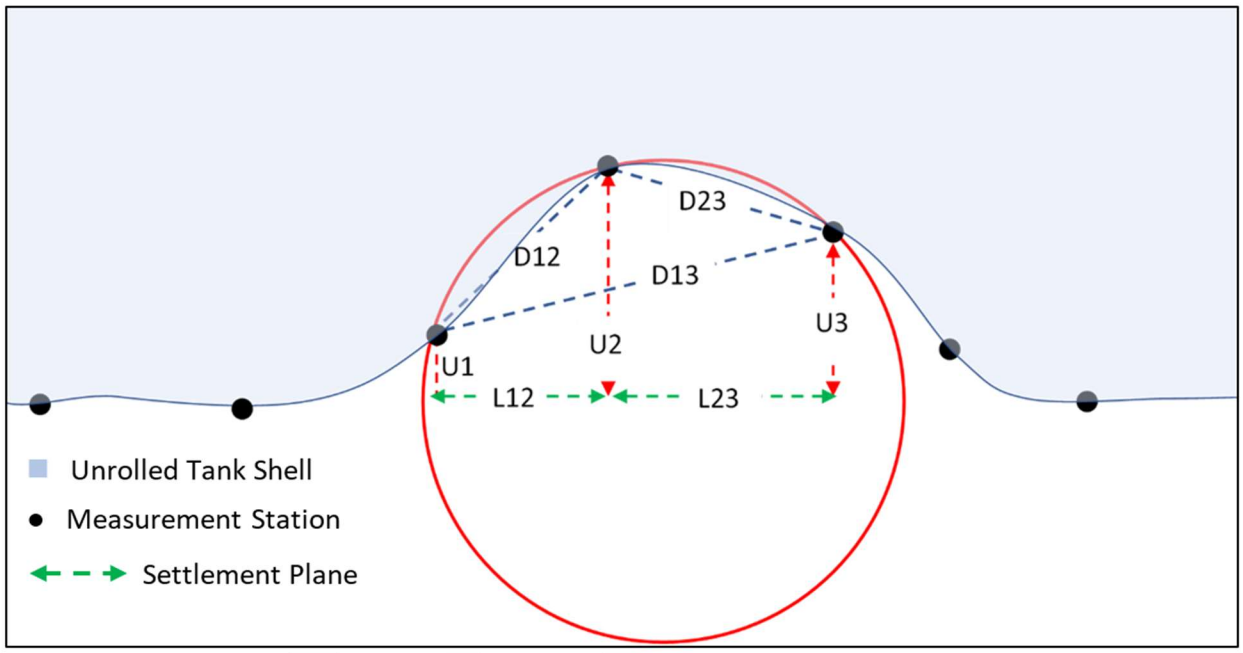

Figure 16. Data for 3-Point Curvature Estimate of a Deflected Section of Tank Shell

Signed curvature, $\kappa = R^{-1}$, is the reciprocal of the radius of curvature at a point on the deflection curve. Referring to

Figure 16, a three-point approximation of this curvature called Menger curvature is,

$$\hat{\kappa} = \frac{2 \cdot \left(L_{12} \cdot \left(U_3 - U_2 \right) - L_{23} \cdot \left(U_2 - U_1 \right) \right)}{d_{12} \cdot d_{23} \cdot d_{13}} \tag{10}$$

When $L_{12} = L_{23} = L$, Equation (10) becomes[11],

$$\hat{\kappa} = L \cdot 2 \cdot \frac{\left(U_1 + U_3 \right) - 2 \cdot U_2}{d_{12} \cdot d_{23} \cdot d_{13}} \tag{11}$$

Distance d_{ij} is the hypotenuse of a right triangle with base L_{ij} and height $U_j - U_i$. In practice,

[11] Factor 2 in the numerator comes from $L_{13} = L_{12} + L_{23} = 2 \cdot L$.

distances between stations exceed 16 feet and differences between out of plane deflections are in the range ±4". Consequently, expressing 4" as 1/3 foot, L_{ij} is, less than 0.022% shorter than d_{ij} , as demonstrated in Equation (12).

$$1 \le \frac{d_{ij}}{L_{ij}} = \frac{\sqrt{L_{ij}^2 + \left(u_j - u_i\right)^2}}{L_{ij}} \le \sqrt{1 + \left(\frac{1/3}{16}\right)^2} = 1.00022\,. \tag{12}$$

Replacing d_{ij} *by* L_{ij} in Equation (10),

$$\begin{aligned} \hat{\kappa} &= L \cdot 2 \cdot \frac{\left(U_1 + U_3\right) - 2 \cdot U_2}{d_{12} \cdot d_{23} \cdot d_{13}} \\ &= 2 \cdot \frac{\left(U_1 + U_3\right) - 2 \cdot U_2}{2L^2} \cdot \left[\frac{L_{12} \cdot L_{23} \cdot L_{13}}{d_{12} \cdot d_{23} \cdot d_{13}}\right] \\ &\cong 2 \cdot \frac{\left(U_1 + U_3\right)/2 - U_2}{L^2} \end{aligned} \tag{13}$$

Equations (12) and (13) imply that the percent error in Equation (13) is,

$$100 \cdot \left(1 - \frac{L_{12} \cdot L_{23} \cdot L_{13}}{d_{12} \cdot d_{23} \cdot d_{13}}\right) \le 100 \cdot \left(1 - \left(1.00022\right)^{-3}\right) = 0.066\%$$

Marr et al. defined out-of-plane deflection[12] (also used in API 653 B.2.2.4) as,

$$S_i = U_i - \frac{U_{i-1} + U_{i+1}}{2} \cong -\frac{\hat{\kappa}_i \cdot L^2}{2} \tag{14}$$

where L is the (uniform) distance (feet) between measurement stations, and out-of-plane deflections, *U*, are also in feet.

Assuming U and L are measured in feet, Marr's criterion for a safe amount of out-of-plane deflection[13] is,

$$S_i \le K \cdot \frac{L^2 \cdot \sigma_f}{H \cdot E} \tag{15}$$

Equivalently,

[12] "S" stands for "sag".

[13] Equation (7) of W. A. Marr, J. A. Ramos, and T. W. Lambe, "Criteria for Settlement of Tanks," *Journal of Geotechnical Engineering*, 108(GT8), August 1982.

$$-\hat{\kappa}_i \le 2 \cdot K \cdot \frac{\sigma_f}{H \cdot E} \tag{16}$$

Where,

K is "(an empirical) constant that includes the nonelastic behavior of the shell material, secondary effects of the tank geometry, and other factors,"

U_i is the deflection in feet of the i[th] elevation from the plane of rigid settlement,

$S_i = U_i - \left(U_{i+1} - U_{i-1}\right)/2$ is sag or "out-of-plane settlement" in feet,

L is arc length between (evenly spaced) measurement points, in feet,

σ_y is the yield strength of the shell material, 36 ksi for A36 steel,

σ_f is the tensile strength of the shell material, 58 ksi for A36 steel,

E is Young's Modulus of the shell material, 29,000 ksi for A36 steel, and

H is tank height, in feet (ft).

Based on data from 38 floating-roof tanks (see Table 5), and 56 cone-roof tanks, Marr recommended $K = 7$; inserting this in equation (15) gives us the final form of Marr's criterion,

$$S_i \le 7 \cdot \frac{L^2 \cdot \sigma_f}{H \cdot E}, \text{ or} \tag{17}$$

$$\hat{\kappa} \le 14 \cdot \frac{\sigma_f}{H \cdot E} \tag{18}$$

Expressed in terms of yield strength[14], σ_y, this is,

$$S_i \le 11 \cdot \frac{L^2 \cdot \sigma_y}{H \cdot E} = S_{\max}, \text{ and} \tag{19}$$

$$\hat{\kappa}_i \le 22 \cdot \frac{\sigma_y}{H \cdot E} = \kappa_{\max} \tag{20}$$

Note that this equation for S_i differs from equation (5) by a factor of 2 – presumably the authors of API 653 introduced this as a factor of safety.

Beam-theoretical predicted stress at the top of the tank is,

$$\sigma_{top} = \kappa \cdot E \cdot \left(H - c\right), \tag{21}$$

where c is the height of the neutral axis above the tank bottom.

[14] Marr's used a safety factor for rupture equal to the ratio of tensile to yields stress, which is taken to be 1.6 in Marr et al.

Consequently, Equations (18) and (21) imply that,

$$\sigma_{top} \le 14 \cdot \frac{\sigma_f}{H \cdot E} \cdot E \cdot (H - c) = 14 \cdot \sigma_f \cdot \left(1 - \frac{c}{H}\right)$$

Since the shell is thicker at the bottom, c < H/2. Consequently, Marr's criterion allows ***predicted stress at the top of the shell to be up to 7 times the ultimate tensile stress without risk of failure***. This can be true if most of the predicted stress is relieved in a cylindrical shell by modes not available to a Euler-Bernoulli beam, or if the beam model overpredicts stresses because it does not take into account the stiffening at the top and the bottom as well as the offset neutral axis. These modes include dimpling of the shell and lateral deflection (ovalization) of the top of the shell (Figure 17).

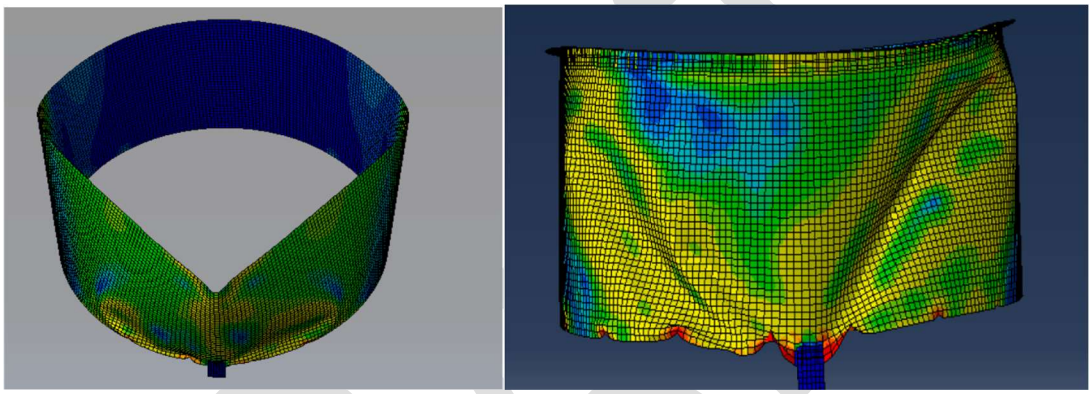

Figure 17. Dimpling and ovalization due to a point stress at the shell bottom[15].

Adapting Marr's Criterion to Laser-Scan Data

When stations are closer than 8 feet, API 653 B.2.2.4 says,

> *… It is acceptable to [use] all measurement points to develop the optimum cosine curve, but only use a subset of these points spaced no further than 32 ft (8 minimum) when calculating* S_i *and* S_{max}*. The points used must include the points furthest from the optimum cosine curve. For example, if 8 points are required, but 16 measurements are taken, and the arc length between measurement points is only 15 ft, calculate the optimum cosine curve using all 16 points, but use only 8 points to calculate* S_i*.*

For example, consider a 272 by 66 ft tank (D x H) was laser scanned at n = 3355 points (stations) around the base of the shell. As an example, let's "thin" the data to L=20 feet between stations.

---

[15] H. Naseri, H. Showkati, T. Zirakian, "Experimental investigation of geometrical and physical behaviors of thin-walled steel tanks subjected to local support settlement," Elsevier, *Structures* 34 (2021) 413–422

The circumference is $272 \cdot \pi \cong 854.5$ ft so there are about 3.96 points per foot or 78 points per 20 feet. Therefore, assuming equal spacing[16], we'd use every 78th point to compute S's, amounting to 43 points in all. API says to start at the largest deviation (U) and retain every 78th point. For example, if U_1 happened to be the largest, we'd use points 1, 79, 157, … 3277, and 3355. We performed this 9 more times with the starting point shifted by L/10, in this case shifted by a count of 8. So, the first shift uses points 9, 89, …,3285, 3363.

Figure 18 shows what that looks like. As a bonus we get an impression of the influence of noise and a "vote" on whether the deflection at 600 feet really exceeds S_{max}: only one out of 10 shifts exceeds S_{max}, so, informally, there's a 10% chance that there is excess deflection.

A weakness of Marr's method is that it is highly sensitive to L, the distance between stations, as illustrated in Figure 19. It appears that the deflection limit (the red dotted line) gets larger with the distance (L) between stations. We'll show later that what is actually happening is that the second difference increasingly underestimates the second derivative and for that reason,

For Marr's method we recommend that laser scanned stations be thinned to $L \cong 20$ ***feet.***

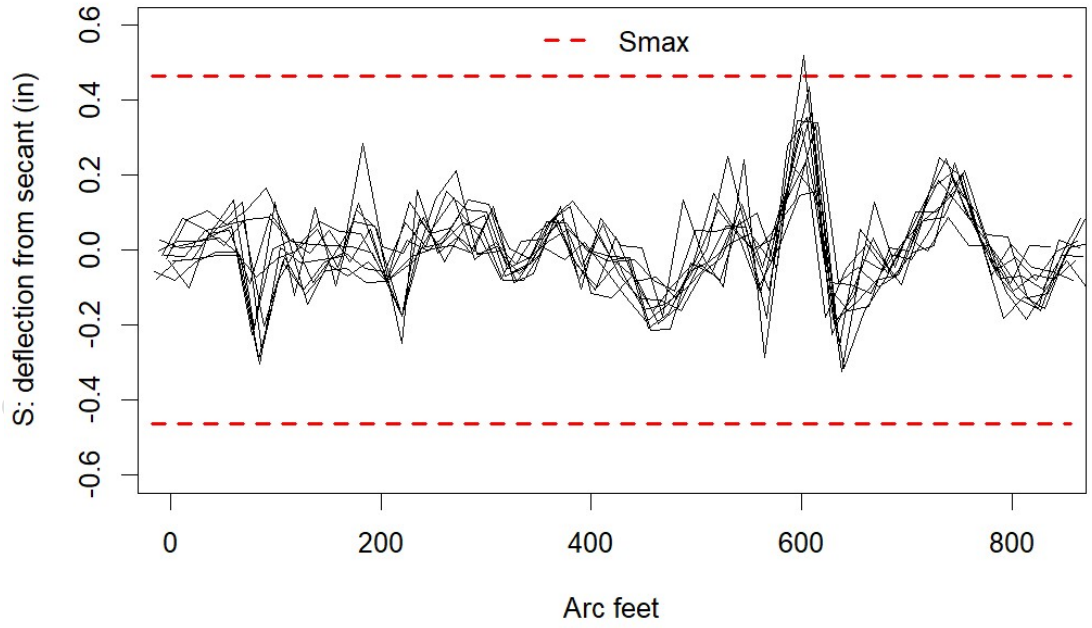

Figure 18. Marr's method with L=20 for laser-scan data.

[16] When spacing is unequal or has gaps points should be selected by distance rather than count.

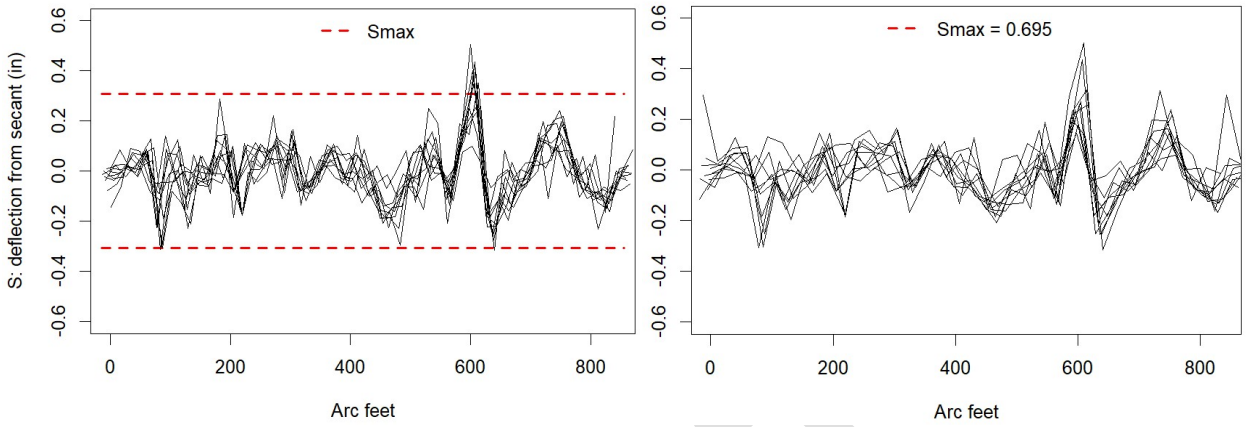

Figure 19. Marr's method with L = 16 feet (left) and 24 feet (right). Note that the dotted red line showing the Smax limit is not visible for L=24 feet.

Why Marr's Method fails for wide spacing, L.

Marr's method assumes that the divided second difference of a function $u(\ell)$ is a good approximation of its second derivative. Since function u is defined around the perimeter of a circle it is a periodic function and can be represented as a Fourier series in amplitude-phase form,

$$u(\ell) = \sum_{k \geq 2} A_k \cdot \cos\left(k \cdot \frac{\ell}{R} - \varphi_k\right) \tag{22}$$

or in cosine-sine form,

$$u(\ell) = \sum_{k \geq 2} a_k \cdot \cos\left(k \cdot \frac{\ell}{R}\right) + b_k \cdot \sin\left(k \cdot \frac{\ell}{R}\right). \tag{23}$$

where ℓ is the arc length (ft) from the origin, R is the diameter, ℓ/R is the angle in radians, k is the order, or harmonic, (cycles per perimeter), A_k is the amplitude of that order, and φ_k is the phase angle. There is no constant or first-order term in equation (23) because these were removed by subtracting the tilt plane. The relationship between the amplitude-phase form and the cosine/sine form is,

$$\begin{aligned} A &= \operatorname{sgn}(a_k) \cdot \sqrt{a_k^{\,2} + b_k^{\,2}}, \text{ and} \\ \varphi &= \arcsin(b_k / a_k) \end{aligned} \tag{24}$$

When equation (23) contains only statistically significant terms we call it a *trigonometric fit* (trig fit, for short).

Figure 19 is a trig fit, $\hat{u}(\ell)$, to the data underlying Figure 18. Figure 20 displays second derivatives and differences in a region around the maximum deflection. The graph shows the second

 Copyright PEMY Consulting, LLC

derivative $d2 = \hat{u}''(\ell)$ and second divided differences $\Delta 2 = \Delta^2(u)/\Delta\ell^2$ at 8 to 32 feet between stations (L). Clearly, the second difference severely underestimates the second derivative for wider spacing. For example, for 32 ft spacing, is can be seen visually that the second finite difference approximation is less than ½ of the true second derivative.

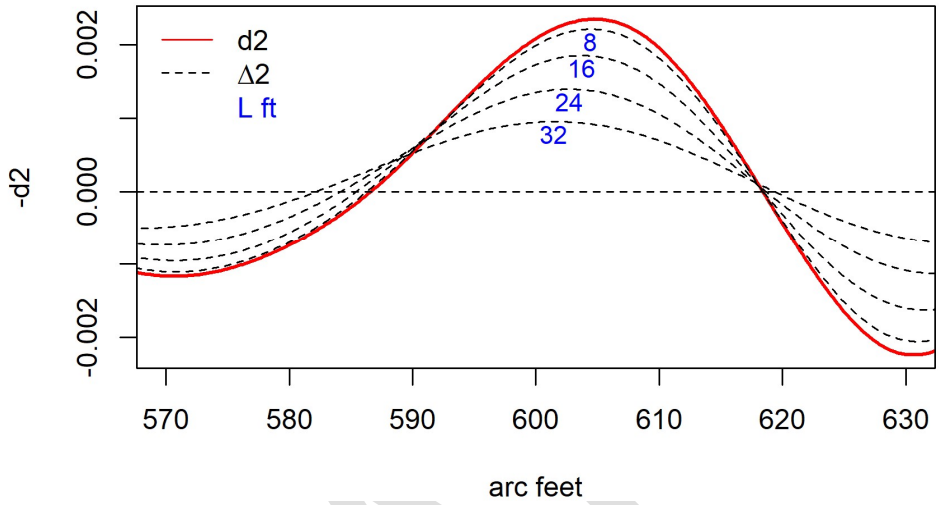

Figure 20. Second difference underestimates second derivative.

More accurate estimation of second derivatives via trigonometric smoothing.

We suggest estimating second derivatives by statistically fitting a finite Fourier series like Equation (22) to the observed deflections from the rigid tilt plane. Cosine terms are only included if they increase the model's overall adjusted R^2, using a method called forward stepwise regression, as described in the section titled *The tilt plane should always be subtracted from raw settlement values*. We analytically calculate the second derivative of the fitted Fourier series to determine the curvature, as opposed to the second difference curvature estimate used by Marr's. We call this the *Trigonometric Regression Method.* In light of our analysis of estimation bias[17] and noise sensitivity, we think that, for laser-scan data, this method is less sensitive to arc length than Marr's original method.

$$\hat{u}''(\ell) = -\sum_{k \geq 2} \left(\frac{k}{R}\right)^2 \cdot \hat{A}_k \cdot \cos\left(k \cdot \frac{\ell}{R} - \hat{\varphi}_k\right) \tag{25}$$

Combining equations (9) and (19) we get *Marr's Criterion with Estimated Derivative*,

$$\hat{u}''(\ell_i) \leq 22 \cdot \frac{\sigma_y}{H \cdot E} = d2_{\max}. \tag{26}$$

[17] Second derivatives of the trigonometric curve are unbiased estimates of its curvature, but the curve itself could be smoother than the true deflection curve.

PEMY Consulting has developed an R application that calculates the criteria discussed in this chapter. Figure 21 shows the trigonometric regression method applied to the data underlying Figure 18.

The advantage of this method is that it is unnecessary to thin the data to arcs of length L.

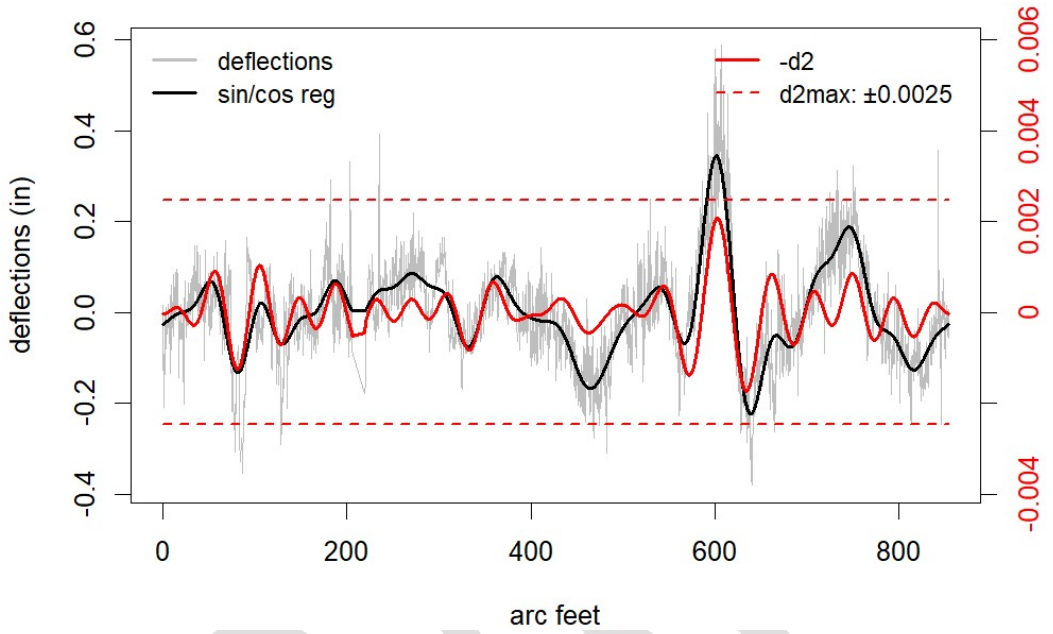

Figure 21. Marr's Criterion with Estimated Second Derivative.

***The trigonometric regression method is compliant with API 653, paragraph B.2.2.4, because Marr et al. explicitly derived their criterion from the equivalent of our Eq.* (9).**

When closely spaced observations are available, trig-reg should be used instead of three-point curvature estimates with thinning. The trig-reg estimate of curvature is unbiased and less susceptible to noise. In addition, it is more precise because it uses all of the observations, not just three points.

DRAFT

Andreani's Method

When finite element analysis (FEA) became computationally practical for tank bottom settlement, Andreani and Carr[18] simulated the stress patterns produced by single folds and developed an empirical model of maximum stress produced by a given strain. The analysis consisted of varying tank height, diameter, type of roof (cone vs open), and type of material (A36, A537 Class 1, and Type 304 SS). For each test case, variations in maximum deflections and settlement arc length were applied; the analysis then looked at resulting strains and out-of-roundness to develop a maximum settlement criterion. This work was incorporated into API 653 as appendix section B.2.2.5.

Andreani's strain measure, also called S_i, is also based on out-of-plane deflections, $U_1,\cdots,U_n$. It is defined as the maximum deflection (U) in an arc bounded by interpolated zeroes. Figure 22 shows out-of-plane deflections (U) at 31 stations[19] around the perimeter of a 272 x 63.6-foot tank.

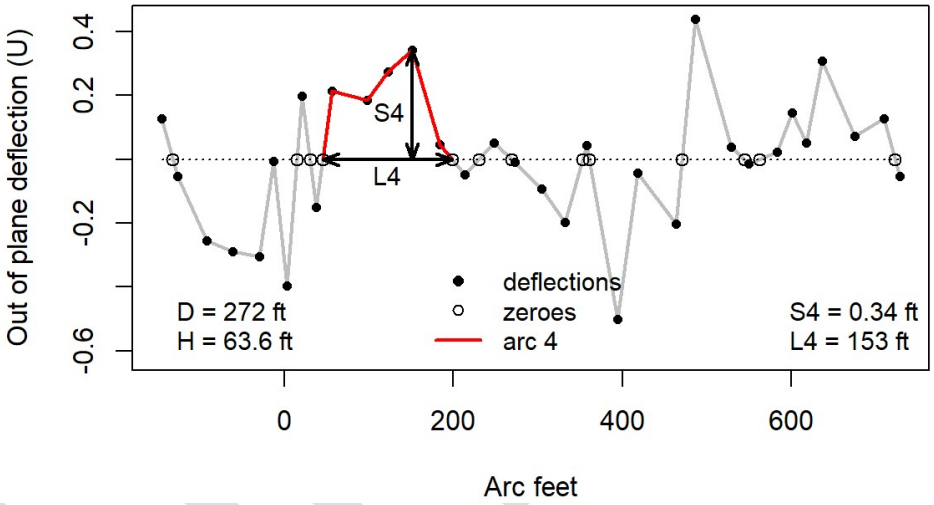

Figure 22. Andreani's Strain Measure, S_i and Arc Length[20] $L_i=S_{arc,i}$

Andreani et al. developed following criterion (also seen in API 653 B.3.2.2):

$$S_i \le K^* \cdot S_{arc,i} \cdot \left(\frac{D}{H}\right) \cdot \left(\frac{\sigma_y}{E}\right) \tag{27}$$

Where K^* is selected from Table 1, and the symbols are,

---

[18] Andreani, J.L., and Carr, N.A. *Study of Out-of-Plane Tank Settlement*, API, Washington, D.C., May 2007.

[19] There are 33 stations in the graph because the rightmost deflections wrap around to the left side of the plot.

[20] Andreani's L is the total arc length whereas Marr's L is the distance between stations, see Equations (28) through (30) for details.

S_i is the absolute value of the maximum deflection in the i[th] arc containing entirely positive or entirely negative deflections from the best-fitting tilt-plane (feet).

K^* is a tabulated value from Table 1, calculated empirically from FEA results that depends on diameter and type of roof,

$S_{arc,i} = L_i$ = settlement arc length, ft = distance between the two zeroes that define the arc.

D = tank diameter, ft

H = tank height, ft

$YS = \sigma_y$ = yield strength, psi

E = Young's Modulus, psi

Andreani's method was calibrated for arcs longer than 20 feet, so if it is applied to laser-scanned data arcs shorter than 20 feet should be ignored.

Figure 23 is the Andreani analysis of the data in Figure 21. The red lines are critical values (the right side of Eq. (27) for arcs at least 20 feet long. The deflection at about 600 feet exceeds the limit and should be further investigated.

For the data in Figure 21, there is general agreement between Marr (Figure 18), Marr with estimated second derivative (Figure 20), and Andreani (Figure 23) that the maximum deflection near arc length 600 ft. is critical or nearly so.

In the next section we demonstrate that Andreani's method corrects the bias shown in Figure 26 that was first noted by D'Orazio and Duncan[21], from which we conclude:

***Andreani's method is more reliable than Marr's method when the separation between stations exceeds 20 feet*.**

[21] D'Orazio, A. M. and James M Duncan, Discussion (of "Criteria for Settlement of Tanks by Marr, Ramos, & Lambe"), *Journal of the Geotechnical Engineering Division*, ASCE, Volume 108 Issue 8 - August 1982.

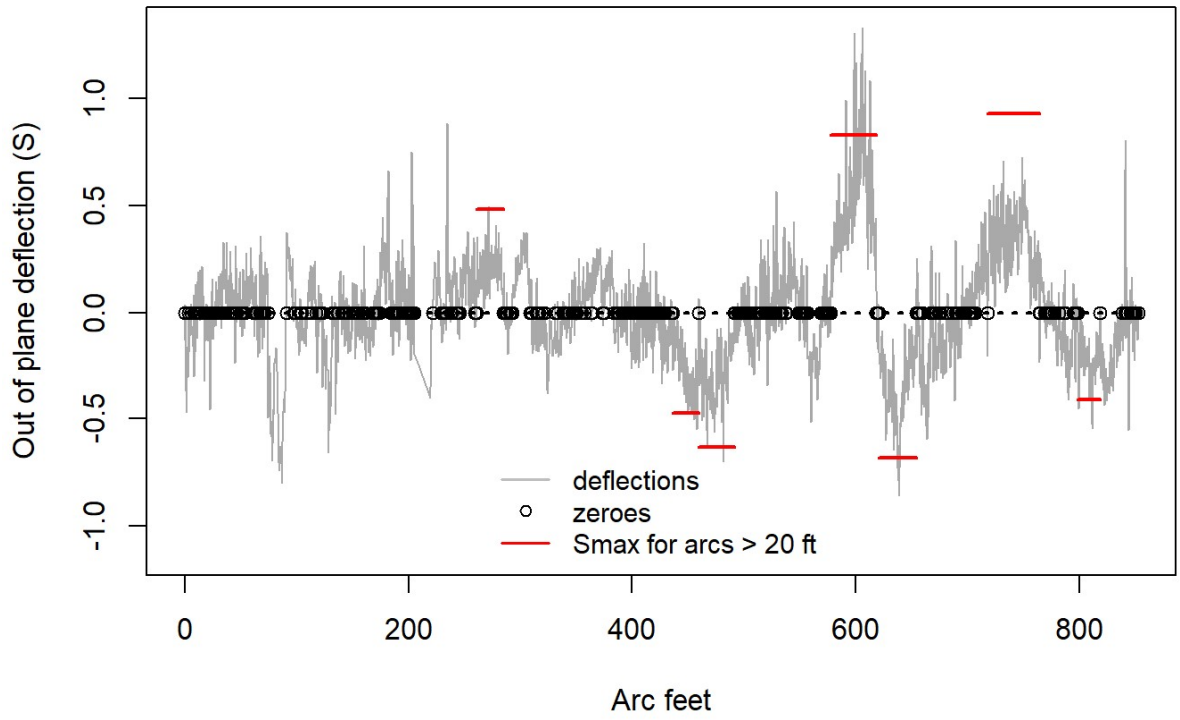

Figure 23. Andreani analysis of laser-scan data.

Comparison of Marr and Andreani Criteria

Referring to Figure 22, let's define a few symbols,

$$\begin{aligned} \ell_{i,left}, \ell_{i,right} &= \text{left and right endpoints of the i}^{\text{th}} \text{ arc} \\ \ell_{i,\max} &= \text{location of max deflection, } U_{i,\max} \\ U_{i,left}, U_{i,right} &= 0 \ (\text{by definition}) \end{aligned} \tag{28}$$

Then we can interpret Andreani's S as a second difference,

$$\begin{aligned} -2 \cdot S &= U_{left} + U_{right} - 2 \cdot U_{\max} \\ &= u\left(\ell_{\max} + L_{right}\right) - 2u\left(\ell_{\max}\right) + u\left(\ell_{\max} - L_{left}\right) + noise \end{aligned} \tag{29}$$

where,

$$\begin{aligned} L_{right} &= \left(\ell_{right} - \ell_{\max}\right) \\ L_{left} &= \left(\ell_{\max} - \ell_{left}\right) \end{aligned} \tag{30}$$

Applying Taylor's expansion we get,

DRAFT

$$
\begin{aligned}
-2 \cdot S &= u\left(\ell_{\max} + L_{right}\right) - 2u\left(\ell_{\max}\right) + u\left(\ell_{\max} - L_{left}\right) + noise \\
&\approx \left(L_{right} - L_{left}\right) u'\left(\ell_{\max}\right) + \frac{\left(L_{right}^2 + L_{left}^2\right)}{2} u''\left(\ell_{\max}\right) \\
&= \tilde{L}^2 \cdot u''\left(\ell_{\max}\right),
\end{aligned}
\tag{31}
$$

where $\tilde{L} = \sqrt{\left(L_{left}^2 + L_{right}^2\right)/2}$ and the first derivative $u'\left(\ell_{\max}\right)$ vanishes at the maximum.

Average separation between the three points is $L = \left(L_{left} + L_{right}\right)/2$ and,

$$
\frac{L^2}{\tilde{L}^2} = \frac{\left(1+\rho\right)^2}{2 \cdot \left(1+\rho^2\right)} \tag{32}
$$

where,

$$
\rho = \frac{\min\left(L_{left}, L_{right}\right)}{\max\left(L_{left}, L_{right}\right)}
$$

For even spacing; i.e., $L_{left} = L_{right}$, we have $L = \tilde{L}$ and $\rho = 1$.

Finally, by combining equations (27) and (31), Andreani's criterion is, approximately,

$$
u''\left(\ell_{\max}\right) \le \left[\frac{\left(1+\rho\right)^2}{2\left(1+\rho^2\right)} \cdot \frac{K^* \cdot D}{2 \cdot L}\right] \cdot \frac{\sigma_y}{H \cdot E} \tag{33}
$$

Whereas, Marr's criterion is

$$
u''\left(\ell_i\right) \le 22 \cdot \frac{\sigma_y}{H \cdot E} \tag{34}
$$

In other words, Andreani replaced Marr's constant multiplier, 22, with a value that depends on diameter, average distance between the three measurement stations used to calculate S, and the ratio of distances to the left and right endpoint of the arc. So, Andreani, in effect, has replaced Marr's multiplier of 22 with,

$$
Andreani's\ implied\ multiplier = \frac{\left(1+\rho\right)^2}{2\left(1+\rho^2\right)} \cdot \frac{K^* \cdot D}{2 \cdot L} \tag{35}
$$

Table 2 lists Andreani's implied multiplier for diameters between 150 and 250 feet, and 16-to-32-foot average separation between the three measurement stations used to compute Marr's deflection measure.

DRAFT

Marr's multiplier, 22, is revealed as the correct multiplier for 16-foot separation between stations in a 180 to 240 foot diameter tank, as is evident in Figure 19. For longer arcs Marr's multiplier is too lenient and Andreani's is the preferred method.

Marr's method is too lenient when measurement stations are more than 16 feet apart - it will have a high rate of false negatives (failures to flag excess strain).

			ρ		
			1.00	0.75	0.50
D	K*	L	Andreani's implied multiplier		
150	4	16	18.75	18.38	16.88
150	4	20	15.00	14.70	13.50
150	4	24	12.50	12.25	11.25
150	4	28	10.71	10.50	9.64
150	4	32	9.38	9.19	8.44
200	3.6	16	22.50	22.05	20.25
200	3.6	20	18.00	17.64	16.20
200	3.6	24	15.00	14.70	13.50
200	3.6	28	12.86	12.60	11.57
200	3.6	32	11.25	11.03	10.13
250	2.4	16	18.75	18.38	16.88
250	2.4	20	15.00	14.70	13.50
250	2.4	24	12.50	12.25	11.25
250	2.4	28	10.71	10.50	9.64
250	2.4	32	9.38	9.19	8.44

Table 2. Andreani's multiplier for Marr's deflection, S.

DRAFT

Andreani's Alternate Method

Andreani et al. thought that the settlement data in Figure 24 did not have a "reliable" tilt plane because $R^2 = 0.617$ is less than 0.90 (see Figure 6). They appear to suggest that the analyst should visually identify *settlement arcs* instead, as in Figure 24. There is no conceptual definition of the term "settlement arc" but API 653 section B.2.2.5.1 does give these instructions,

> a) The actual settlement [not deflections from a tilt plane] is plotted using points around the tank circumference as the abscissa.
>
> b) An initial settlement arc length and maximum settlement is determined from the points on the plotted data that indicate a change in direction of settlement slope [see Figure 24].
>
> [Judging from Figure 24, "change in direction" appears to mean a settlement arc is defined by places where the slope changes sign, in other words, at local maxima and minima. For example, S_{arc5} is bounded by local maxima at stations 2 and 10, and has a local minimum at station 6. The arc with greatest absolute deflection is, for unknown reasons, not marked in API 653 Figure B4: it is the dotted red line in Figure 24 that runs from station 5 to station 11 with maximum deflection at station 9.]
>
> c) Additional settlement measurement points may be needed halfway between the points indicating a change in direction of the settlement slope to further refine the settlement arc length and location and magnitude of maximum settlement.
>
> d) Step c) may need to be repeated. The best estimate of the settlement arc length and maximum settlement shall be considered in the procedure given in B.3.2.2 (see Equation (27))

Figure 25 is our rendition of Andreani's standard analysis of deflections from the tilt-plane. Arcs identified by the standard analysis (API 653 Section B.2.2.5) are shown as black arrows and alternate arcs identified by steps a) – d) are shown as red lines. The alternate analysis missed both positive-going arcs (1 and 3), which is a serious error – in beam theory, it is the positive-going arcs that produce tensile stress in the shell above them.

DRAFT

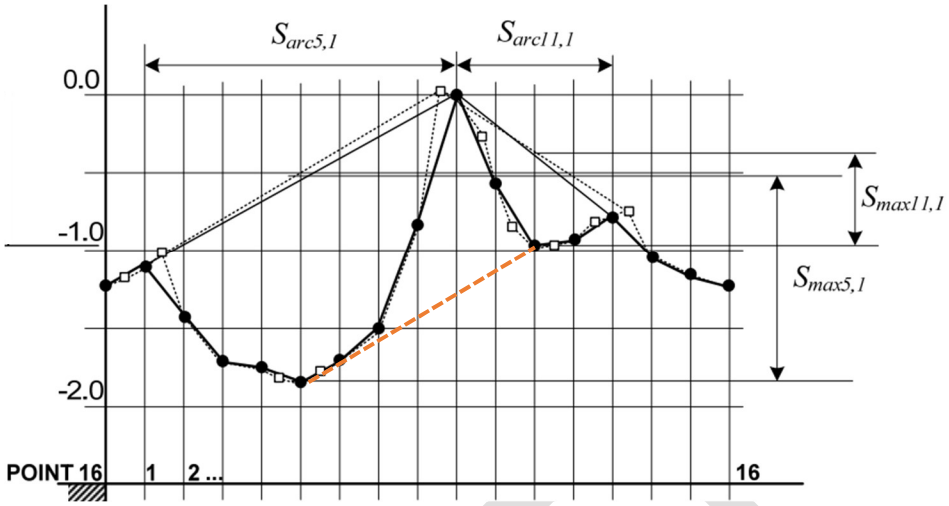

Figure 24. API 653 Figure B.4.

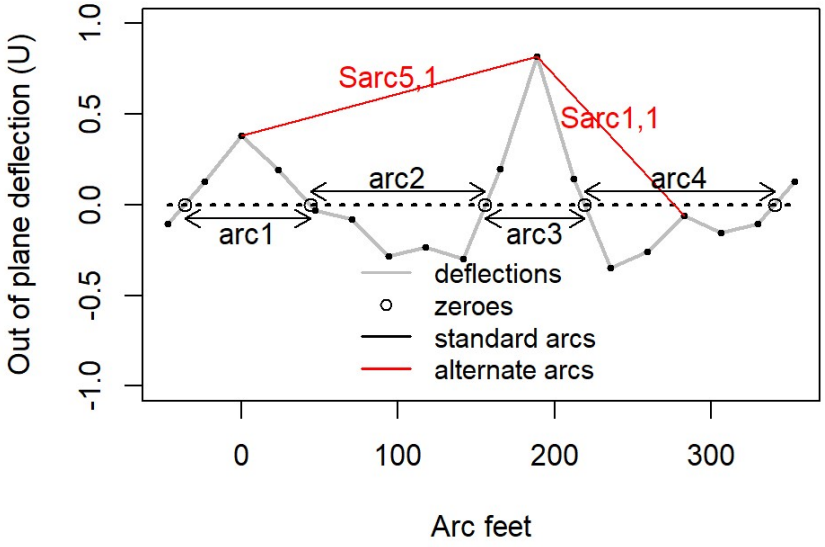

Figure 25. Andreani Standard and Alternate Arcs.

Andreani's standard method based on deflections from the best fitting tilt plane is better calibrated than Marr's method, which is subject to increasing bias as the arc length $(2 \cdot L)$ increases. Andreani's alternate method, based on identifying local maxima and minima, is demonstrably subjective (see the missed arc in Figure 24) and would be even more so for laser-scan data like Figure 23. In any case it is never necessary because it should always be permissible to work with deflections from a fitted tilt plane.

Andreani's standard method is better calibrated than Marr's. Do not use Andreani's alternate method: always use deflections (U) with the tilt plane removed.

Comments on Differential Settlement.

We have discussed the two differential settlement analyses sanctioned by API 653 Appendix B. The first, Marr's method, is based on Euler-Bernoulli beam theory and a divided second difference estimate of the second derivative or curvature. We have shown that the second difference estimate can be badly biased if the distance between stations, L, is longer than 20 feet. We also showed that it has less than a 3-sigma signal to noise ratio when RMS noise is 0.25 inch and L is shorter than 20 feet.

We conclude therefore that Marr's method is generally unreliable but that it can be made more reliable by replacing Marr's strain estimate (S) with the analytical second derivative of a trigonometric fit (finite Fourier series). We recommend running and reporting the Trig Fit method in addition to Marr's second difference method.

A second stress analysis method developed by Andreani, et al., is derived from finite-element modelling of simple folds across the tank bottom. It was calibrated to a limiting strain of 3%, based on the API 579 fitness for service criterion and is therefore one step closer to the gold standard. Andreani's finite element analysis looked only at single folds at different arc lengths but is based on a more realistic model than Marr's method. Unlike Marr's method, it is accurate over a wide range of arc lengths.

API 653 section B.2.2.5 gives this advice:

> *If … the maximum out-of-plane settlement determined in accordance with B.3.2.1 (Marr's method) is exceeded, the procedures given in this section (Andreani's method) may be used in lieu of more rigorous analysis or repair*

We have demonstrated that this advice has it backward: Marr's method is too lenient and will sometimes miss overstressed points that are identified by Andreani's method. Instead, we recommend that a settlement analysis consist of 1) Andreani's standard analysis, then 2) Marr's analysis, if measurement stations are separated by 16 to 20 feet, and then 3) the Trig-Reg method, when measurements are closely spaced. A tank gets a clean bill of health only if both Andreani's and Marr's/Trig-reg analyses are negative (do not indicate overstress).

All of these analyses – Marr, Andreani, and Trig-Reg – are screening tests to identify possible excess stress. The gold standard is finite element analysis.

DRAFT

References

1. James S. Clarke, *Recent Tank Bottom and Foundation Problems*, Esso Research and Engineering Co., Florham Park, N.J., 1971; Phil Smith, Texaco.
2. Andreani, J.L., and Carr, N.A. *Study of Out-of-Plane Tank Settlement*, API, Washington, D.C., May 2007.
3. W. A. Marr, J. A. Ramos, and T. W. Lambe, "Criteria for Settlement of Tanks," *Journal of Geotechnical Engineering*, 108(GT8), August 1982.
4. American Petroleum Institute, API Standard 653, 5th Ed., Washington, 2014, Addendum 2, 2020.
5. H. Naseri, H. Showkati, T. Zirakian, "Experimental investigation of geometrical and physical behaviors of thin-walled steel tanks subjected to local support settlement," Elsevier, *Structures* 34 (2021) 413–422
6. D'Orazio, A. M. and James M Duncan, Discussion (of "Criteria for Settlement of Tanks by Marr, Ramos, & Lambe"), *Journal of the Geotechnical Engineering Division*, ASCE, Volume 108 Issue 8 - August 1982.
7. Z. Malik, J. Morton, and C. Ruiz, "Ovalization of Cylindrical Tanks as a Result of Foundation Settlement," *Journal of Strain Analysis*, 12(4):339–348 (1977).
8. Timothy B. D'Orazio and James M. Duncan, "Differential Settlements in Steel Tanks," *Journal of Geotechnical Engineering*, 113(9), September 1987.
9. S. Timeshenko, *Theory of Plates and Shells*, table 82, 2d ed., McGraw-Hill, New York, 1959.

Figures

Figure 1. Rigid Settlement without Tilt 5
Figure 2. Settlement with Rigid Tilt 7
Figure 3. An example of how a cosine curve looks like a tilted circle in 3D. 8
Figure 4. Translation *s* in the Z-axis with rotation δ about the y-axis. 8
Figure 5. Left: Excel plot of Settlement and Tilted Plane. Right: Residual Deviations from Plane. 9
Figure 6. Planar tilt for Andreani's example 2. The complement of the *p*-value, 1-p = 0.998, is the analyst's *confidence* in saying "the tilt angle is not zero." 10
Figure 7. The effects of increasing angular distortion. 11
Figure 8. From top to bottom, curves increase in number of modes from 1 to 2 to 3. Curves on the left have phase angle set to 0; Curves on the right have their highest frequency mode shifted 90 degrees to the right (+1.5708 radians). 13
Figure 9. A 1-mode cosine fit to settlement data. It could be improved… 14
Figure 10. A 2-mode cosine fit to settlement data. An improvement over the 1-mode fit. 15
Figure 11. Left: the settlement data used in Figure 9 and Figure 10 shown in 3D. Right: the 1-mode (in red) and 2-mode (in blue) cosine fit shown in 3D. 15
Figure 12. The 3-mode cosine fits the best for this settlement data. 16

DRAFT

Figure 13. Deflections (U) from plane of rigid tilt. 20
Figure 14. Deflections, U, from tilt plane and a hypothetical true deflection curve, $u(\ell)$ 22
Figure 15. Unrolled tank bottom showing Radius of curvature of an out-of-plane deflection.... 22
Figure 16. Data for 3-Point Curvature Estimate of a Deflected Section of Tank Shell 23
Figure 17. Dimpling and ovalization due to a point stress at the shell bottom. 26
Figure 18. Marr's method with L=20 for laser-scan data. 27
Figure 19. Marr's method with L = 16 feet (left) and 24 feet (right). Note that the dotted red line showing the Smax limit is not visible for L=24 feet. 28
Figure 20. Second difference underestimates second derivative. 29
Figure 21. Marr's Criterion with Estimated Second Derivative. 30
Figure 22. Andreani's Strain Measure, S_i and Arc Length $L_i=S_{arc,i}$ 31
Figure 23. Andreani analysis of laser-scan data. 33
Figure 24. API 653 Figure B.4. 37
Figure 25. Andreani Standard and Alternate Arcs. 37
Figure 26. Computed lower bound on K for 38 Floating-Roof tanks. 43

DRAFT

Appendix A. Commentary on the Marr Method

Effect of Measurement Error, Roughness, and Spacing on the Marr Method

Using the "signal plus noise" model in Equation (8), observed deflection can be written as true deflection plus noise. Noise consists of measurement error plus intrinsic roughness: welds, dings, patches, etc. Observed deflections U are true deflection plus noise, $U = u(\ell) + e$

$$\begin{aligned} S_i &= U_i - (U_{i+1} + U_{i-1})/2 \\ &= \left[u(\ell_i) - (u(\ell_{i+1}) + u(\ell_{i-1}))/2\right] + \left[e_i - (e_{i+1} + e_{i-1})/2\right] \\ &= [\text{true deflection}] + [\text{noise}] \end{aligned} \tag{36}$$

Assuming that noise is random with standard deviation sd_e, the standard deviation of an out-of-plane deflection is,

$$sd(S_i) = sd(-0.5 \cdot e_{i+1} + e_i - 0.5 \cdot e_{i-1}) = sd_e \cdot \sqrt{1.5} \tag{37}$$

Controlling false positives and false negatives requires that the noise component of S_i be much smaller than the critical value for S, S_{max}

(38)

$$sd_e << \frac{11 \cdot \sigma_y}{E \cdot \sqrt{1.5}} = \frac{L^2}{H} \cdot 0.0112 \tag{39}$$

Operating Characteristic: Probability of a Positive Test for Over-Strain

If noise is Gaussian, the probability of a positive test for over-strain is,

$$\begin{aligned} P(S > S_{\max}) &= P\left(\frac{S - \mu_S}{sd_S} > \frac{S_{\max} - \mu_S}{sd_S}\right) \\ &= P\left(Z > \frac{S_{\max}}{sd_S} \cdot \left(1 - \frac{\mu_S}{S_{\max}}\right)\right) \\ &= P(Z > SNR \cdot SM) \end{aligned} \tag{40}$$

where, SNR is the Signal to Noise Ratio, and SM is the Safety Margin; i.e., the relative distance of true strain μ_S from maximum permitted strain S_{max}

DRAFT

Table 3 shows the effect of SNR and SM on false positives[22] and false negatives[23].

For example, if true stress is 20% below Smax (SM = 0.2) the false positive rate is 12% for SNR=6 sigma and 27% for SNR=3 sigma, with noisy data (SNR=3) 27% of tests will be false positives and 73% will be true negatives. An acceptable level of false positives depends on a cost-benefit analysis of the protocol for following up an apparent positive. Alternately, if true stress is 30% above the limit, Smax, and SNR=3 sigma, there will be 18% false negatives and 82% true positives. An acceptable level of false negatives depends on a cost benefit analysis of protocol for following up an apparent negative.

SM	SNR = 6	SNR=3	
0.5	0	7	% False Positive
0.4	1	12	
0.3	4	18	
0.2	12	27	
0.1	27	38	
0	50	50	
-0.1	27	38	% False Negative
-0.2	12	27	
-0.3	4	18	
-0.4	1	12	
-0.5	0	7	

Table 3. Effect of Signal-to-noise Ratio on False Positive & Negative Rates.

Clearly it is desirable to reduce both false positive and negative rates. That requires reducing noise. Table 3 suggests that a signal to noise ratio at least 6 is needed to avoid excess false positives. then shows the maximum permissible noise standard deviation required to achieve given signal to noise ratios. We shall see that there are strategies for reducing SNR.

Mitigating the Signal to Noise Ratio.

Noise is a combination of intrinsic roughness[24] and measurement error and probably cannot be reduced below .25 inch. Table 4 indicates that 5 sigma or better SNR is out of reach for L less than 20 feet, and, apparently the bigger L is the better. We shall learn that this is counterbalanced by increasing bias in the 3-point curvature estimate as L increases.

It seems, therefore that for methods based on 3-point curvature estimates, the sweet spot between noise and bias is at L = 20 feet. We will show later that there is a more sophisticated

[22] A false positive occurs if the true sag, μ_S is less than S_{max} but observed sag, S, is above S_{max}

[23] False negatives can happen when the tank is truly over the stress limit (SM <0) but observed stress is less than Smax.

[24] Intrinsic roughness due to overlapping plates etc. is ± 0.25

curvature estimate that gets around this problem if the distance between measurement stations is very small, as with laser-scan data.

	H = 40 ft				H = 50 ft			
	SNR				SNR			
L ft	3	4	5	6	3	4	5	6
16	0.29	0.22	0.17	0.14	0.23	0.17	0.14	0.12
20	0.45	0.34	0.27	0.22	0.36	0.27	0.22	0.18
24	0.65	0.49	0.39	0.32	0.52	0.39	0.31	0.26
28	0.88	0.66	0.53	0.44	0.71	0.53	0.42	0.35
32	1.15	0.86	0.69	0.58	0.92	0.69	0.55	0.46
36	1.46	1.09	0.87	0.73	1.17	0.87	0.70	0.58

Table 4. Maximum Permissible Noise Standard Deviation (inches) for Given SNR, L, and H

Marr et al.'s K value Does Not Adjust for Bias Caused by Large L

Marr, et al., computed lower bounds for factor K using data from 38 floating-roof and more than 60 cone-roof tanks that had not ruptured. The logic is that the stress observed in an intact tank must be less than the failure stress. Rearranging equation (15) implies that for all 36 tanks (t) in the calibration set,

$$K > K_{t,observed} = \frac{S_t}{L_t^2} \cdot \frac{H_t \cdot E}{\sigma_f} \tag{41}$$

Observed K values are listed in Table 5 and are plotted against arc length (L) in Figure 26. The red curve is logically a lower bound on K because the 38 tanks had not ruptured but would have ruptured at some higher value of K.

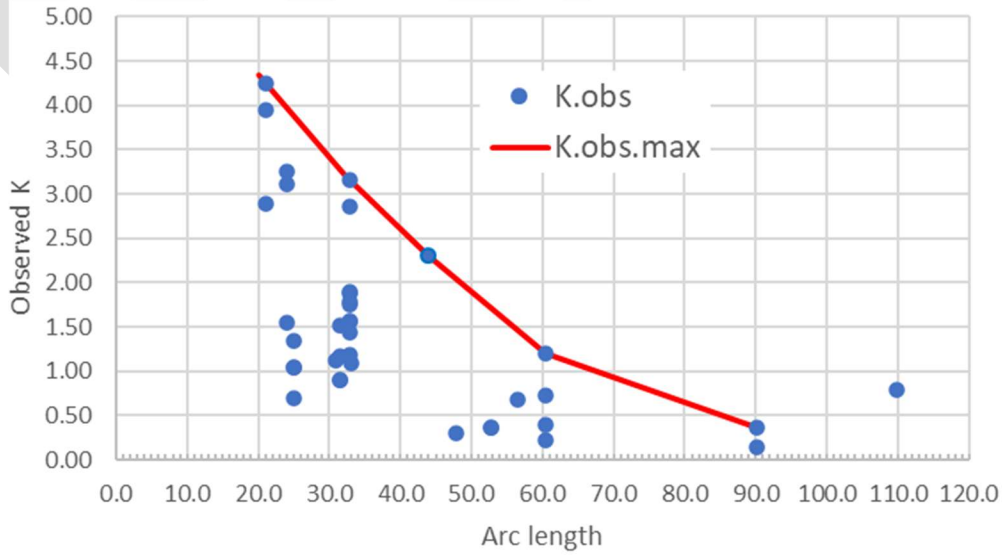

Figure 26. Computed lower bound on K for 38 Floating-Roof tanks.

Copyright PEMY Consulting, LLC

D'Orazio and Duncan[25], pointed out that K decreases quadratically as arc length increases, as shown in Figure 26. They reasoned that noise standard deviation, sd_e, is leveraged by L^{-2}, making $K_{observed}$ more dispersed for small L-values. That might account for some of the decrease, but we have found that the true explanation is the fact that the second divided difference is a biased estimate of the second derivative (see Figure 20).

In the section titled *Adapting Marr's Criterion to Laser-Scan Data*, we demonstrate that the pattern in Figure 26 comes from using an approximation for the second derivative and, consequently, factor K should be a function of the distance *L* between measurement stations.

tank	*Diam*	*Height*	*L arc*	*S.obs*	*K.obs*	*tank*	*Diam*	*Height*	*L arc*	*S.obs*	*K.obs*
1	133.5	55.1	21.0	0.0207	4.25	20	209.6	60.0	32.8	0.0191	1.75
2	133.5	55.1	21.0	0.0193	3.95	21	209.6	60.0	32.8	0.0205	1.88
3	133.5	55.1	21.0	0.0141	2.89	22	209.6	60.0	32.8	0.0195	1.79
4	152.6	54.8	24.0	0.0099	1.55	23	209.6	60.0	32.8	0.0170	1.56
5	152.6	54.8	24.0	0.0199	3.12	24	209.6	60.0	32.8	0.0130	1.19
6	152.6	54.8	24.0	0.0208	3.26	25	209.6	60.0	32.8	0.0156	1.43
7	80.1	42.0	25.1	0.0095	1.04	26	169.0	47.9	33.1	0.0151	1.08
8	96.1	42.0	25.1	0.0095	1.04	27	167.3	48.6	44.0	0.0558	2.30
9	80.1	54.1	25.1	0.0095	1.34	28	244.4	47.9	47.9	0.0087	0.30
10	80.1	42.0	25.1	0.0064	0.70	29	67.3	39.4	52.8	0.0159	0.37
11	315.6	72.2	30.8	0.0090	1.13	30	67.3	39.4	52.8	0.0159	0.37
12	219.8	54.1	31.5	0.0130	1.17	31	144.4	54.1	56.4	0.0244	0.68
13	219.8	54.1	31.5	0.0100	0.90	32	229.7	48.6	60.4	0.0180	0.39
14	219.8	54.1	31.5	0.0100	0.90	33	229.7	48.6	60.4	0.0551	1.20
15	180.4	54.1	31.5	0.0170	1.52	34	229.7	48.6	60.4	0.0330	0.72
16	209.6	60.0	32.8	0.0170	1.56	35	229.7	48.6	60.4	0.0100	0.22
17	209.6	60.0	32.8	0.0207	1.89	36	229.7	48.6	90.2	0.0140	0.14
18	209.6	60.0	32.8	0.0313	2.86	37	229.7	45.9	90.2	0.0400	0.37
19	209.6	60.0	32.8	0.0345	3.16	38	139.8	48.2	109.9	0.1218	0.80

Table 5. Marr, et al.'s Calibration Set (adapted from their Figure 6, all dimensions in feet).

[25] D'Orazio, A. M. and James M Duncan, Discussion (of "Criteria for Settlement of Tanks by Marr, Ramos, & Lambe"), *Journal of the Geotechnical Engineering Division*, ASCE, Volume 108 Issue 8 - August 1982.